

國立交通大學

機械工程學系
碩士論文

Silicon Oxide (SiO_x) Film Deposition Using Radio-Frequency

Atmospheric-Pressure Plasma Jet With a Spiral Electrode

利用螺旋式電極的常壓射頻電漿束鍍製氧化矽薄膜之研究



研究生：呂其璋

指導教授：吳宗信 博士

中華民國九十九年七月

利用螺旋式電極的常壓射頻電漿束鍍製氧化矽薄膜之研究

Silicon Oxide (SiO_x) Film Deposition Using Radio-Frequency

Atmospheric-Pressure Plasma Jet With a Spiral Electrode

研 究 生：呂其璋

Student : Chi-Chang Lu

指 導 教 授：吳宗信博士

Advisor : Dr. Jong-Shinn Wu



**Submitted to Department of Mechanical Engineering
College of Engineering
National Chiao Tung University
in Partial Fulfillment of the Requirements
for the degree of
Master in
Mechanical Engineering**

July 2010

Hsinchu, Taiwan

西元二零一零年七月

利用螺旋式電極的常壓射頻電漿束鍍製氧化矽薄膜之研究

學生：呂其璋

指導教授：吳宗信 博士

國立交通大學機械工程學系

摘要

本文係探討以同軸式耦合射頻常壓電漿系統進行鍍製氧化矽(SiO_x)薄膜技術之研究。利用同軸式耦合射頻電漿，放電氣體為混合的氬氣與氧氣，電源頻率為13.56 MHz，在一大氣壓條件下產生電漿源。在使用石英管包覆內層螺旋式電極下，氬氣可以混合高比例的氧氣(10%) 並產生穩定且無電弧的電漿。利用本系統進行鍍製氧化矽薄膜，使用六甲基二矽氧烷 (Hexamethyldisiloxane, HMDSO) 做為沈積薄膜之前驅物，並利用氬氣做為前驅物的載體，將前驅物導入後放電區域沈積氧化矽薄膜於矽基材上。改變不同實驗參數來探討薄膜特性，包括處理次數、處理距離(3-7.5 mm)、輸入功率(35-50W)、氧氣濃度(0-10 %)及基板溫度(25-300 °C)。由實驗結果得知，鍍膜沈積速率會隨著處理次數、輸入功率及氧氣濃度增加而增加；隨著處理距離、基板溫度增加而減少。並進一步去探討在不同的氧氣濃度及基板溫度下進行鍍膜，薄膜特性的變化。

在輸入功率為50 W、基板溫度為300 °C、處理距離為5 mm的實驗參數下進行鍍

膜，氫氣電漿在無氧氣添加下，鍍膜速率為37.5 nm/min，若氧氣濃度增加至0.8%，鍍膜速率會明顯上升至275 nm/min 但是在氧氣濃度增加至2%以上，發現會有高孔性的結構產生。由FTIR及XPS量測結果發現，薄膜中碳的成份會隨著基板溫度增加而減少。在較高的基板溫度下進行鍍膜可以降低鍍膜速率，並減少薄膜孔性程度，且提高薄膜硬度。

總結來說，在氫氧電漿混合適當比例的氧氣下，我們可成功於後放電區沈積氧化矽薄膜，並且在不同實驗參數下討論薄膜的特性。同時在論文的最終節列出建議未來應進行的研究。




Silicon Oxide (SiO_x) Film Deposition Using Radio-Frequency Atmospheric-Pressure Plasma Jet With a Spiral Electrode

Student : Chi-Chang Lu

Advisor : Dr. Jong-Shinn Wu

**Department of Mechanical Engineering
National Chiao Tung University**

Abstract



Thin film deposition of silicon oxide (SiO_x) using a radio-frequency (13.56 MHz) coaxial argon atmospheric-pressure plasma jet (RF-APPJ) has been investigated experimentally in this thesis. A stable, arc-free swirling APPJ was produced with a spiral powered electrode covered by a quartz tube, which makes the addition of oxygen (up to 10%) possible without extinguishing the discharge. This APPJ was employed to deposit silicon oxide thin films using a precursor, hexamethyldisiloxane (HMDSO), diluted in an argon carrier gas, into the post-discharge region. Test conditions included variations of treatment passes, input power (35-50 W), treatment distances (3-7.5 mm), oxygen additions (0-10%), and substrate temperatures (25-300 °C). Results show that deposition rate increased with increasing treatment passes, input power, oxygen addition and

decreased with increasing substrate temperatures and treatment distances. The variation of oxygen addition and substrate temperature greatly affected the properties of silicon oxide thin films.

The deposition rate of the silicon oxide thin film was 37.5 nm/min using pure argon plasma with 50 W RF power, 300 °C substrate temperature and 5 mm treatment distance.

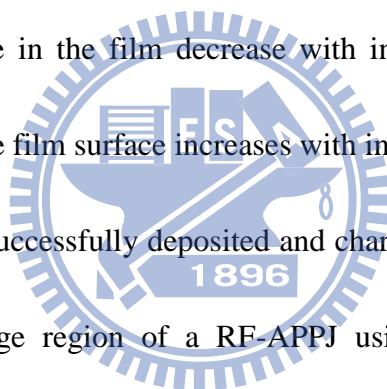
When oxygen addition increases to 0.8%, the deposition rate increases to 275 nm/min.

However, oxygen addition is more than 2%, highly porous, particle-like structure was formed. FTIR and XPS measurements show that quantity of carbon atoms, the degree of porosity and deposition rate in the film decrease with increasing substrate temperature.

However, the hardness of the film surface increases with increasing substrate temperature.

In summary, we have successfully deposited and characterized the silicon oxide films formed in the post-discharge region of a RF-APPJ using argon mixed with oxygen.

Recommendations for the future study are also outlined at the end of the thesis.



致謝

在交大求學的這兩年過程中，要特別感謝辛勞的指導教授吳宗信博士，提供完善的學習環境及優秀的研究團隊，吳教授的直執與熱忱影響我們對於研究的態度，細心教導並無保留的傳達所學經驗，在此，僅以此文向恩師致以最衷心的感謝。同時也感謝口試委員許鈺宗老師、吳建一老師和廖國基老師細心審閱並給予意見，讓論文更加完善。

此外要感謝吳教授實驗室的所有人，江明鴻學長、博士後研究郭啟良博士及林逸民學長，在我研究過程中，提供了許多寶貴的經驗；也感謝捷祭、正勤、昆樸、孟樺、雅茹、沅明、凱文、必任、與子豪等學長學姐，在各方面給予我的幫助及分享許多學習經驗；和我同儕兩年的致友皓遠同學，在研究與生活中相互勉勵，一起為實驗室打拼；以及親愛的學弟們，宜偉、曄能、瑞祥、伯村和志東等，在實驗上的幫忙不餘於力。在此也感謝這兩年來在生活上給予我鼓勵的朋友，交大的信宏和派宣，清華的昶宏和昱誠，以及樂生青年志工及小朋友們。

最後，要感謝總是會燉好雞湯等著我回家吃飯的家人。當我遇到挫折和困難，不管在何時，他們總是為我加油打氣。非常感謝他們一路的栽培、鼓勵與關心，僅將此文獻給我輩最敬愛的家人。

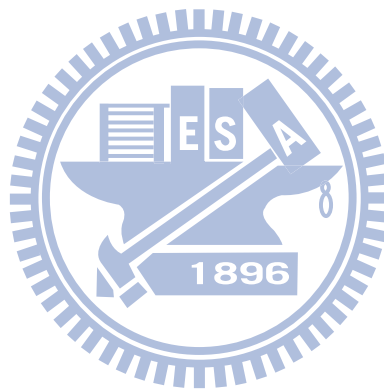
其璋

2010 七月 于新竹

Table of Contents

摘要.....	i
Abstract.....	iii
致謝.....	v
Table of Contents	vi
List of Tables.....	viii
List of Figures.....	ix
Nomenclature.....	xii
Chapter 1 Introduction.....	1
1.1 Motivation	1
1.2 Background.....	2
1.2.1 Deposition of Silicon Oxide (SiO _x) Films and Its Applications.....	2
1.2.2 Classification of Atmospheric-Pressure Discharges.....	4
1.3 Literature Review	6
1.3.1 Deposition of SiO _x Films at Atmospheric-Pressure Condition	6
1.4 Specific Objectives and Organization of the Thesis.....	9
Chapter 2 Experimental Methods.....	11
2.1 Experimental Facility.....	11
2.1.1 APPJ System.....	12
2.1.2 RF Power Supply.....	12
2.1.3 Matching Box	13
2.1.4 Gas Feeding System	13
2.2 Experimental Instrumentation	14
2.2.1 V-I Probe for Electrical Property Measurements.....	14
2.2.2 OES (Optical Emission Spectroscopy) for Species Identification Measurements.....	15
2.2.3 Scanning Electron Microscope (SEM) for Cross-section Morphology Observation of Thin Film	15
2.2.4 Atomic Force Microscope (AFM) for Surface Topology Observation	16
2.2.5 Fourier Transform Infrared Spectroscopy (FTIR) for Surface Bonding Identification.....	16
2.2.6 X-ray Photoelectron Spectroscopy (XPS) for Surface Element Analysis and Bonding Identification.....	16
2.2.7 Contact Angle Measurement Device	17
2.2.8 Pencil Hardness Test.....	17
2.3 Experimental Procedures and Test Conditions	18
Chapter 3 Results and Discussion	20

3.1 Electrical Characterization of the APPJ System.....	20
3.2 Visual Observation and Optical Emission Spectral Analysis of APPJ	22
3.3 Surface Morphology and Deposition Rate of Thin Film.....	23
3.3.1 Effect of Number of Treatment Passes	24
3.3.2 Effect of Input Power	24
3.3.3 Effect of Treatment Distance	25
3.3.4 Effect of Substrate Temperature	26
3.3.5 Effect of Oxygen Concentration in the Discharge.....	27
3.4 Bond Structure Analysis by FTIR	28
3.5 Surface Composition Analysis by XPS	30
3.6 Contact Angle Measurements	31
Chapter 4 Concluding Remarks.....	33
4.1 Summary.....	33
4.2 Recommendations of Future Work	34
References	35



List of Tables

Table 1 Subdivision of plasmas [Hippler <i>et al.</i> , 2008].	41
Table 2 Comparison of plasmas sources [Schutz <i>et al.</i> , 1998].	42
Table 3 Density of oxygen species in the plasma discharge [Schutz <i>et al.</i> , 1998].	42
Table 4 Summary of important features for SiO _x thin films deposition using APPJ at remote region.	43
Table 5 Properties of HMDSO.	43
Table 6 Summary of the instrumentation.	44
Table 7 Test conditions of RF-APPJ for SiO _x deposition.	45
Table 8 Pencil hardness results of SiO _x films.	45
Table 9 Elemental composition of SiO _x under various oxygen concentrations.	46
Table 10 Elemental composition of SiO _x under various substrate temperatures.	46

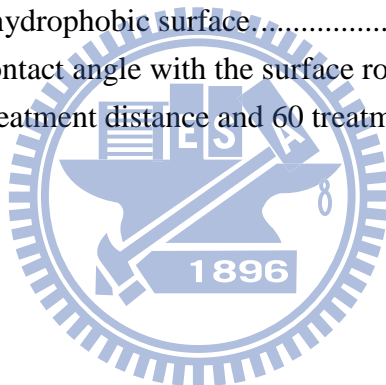


List of Figures

Figure 1.1 Schematic representation of the PECVD reaction process [Konuma, 2005].....	47
Figure 1.2 The system configuration for LP-PECVD reactor [Pai <i>et al.</i> , 1990].	47
Figure 1.3 Types of atmospheric pressure plasma. (a) Transferred arc; (b) Corona discharge; (c) Dielectric barrier discharge; (d) Plasma jet [Schutz <i>et al.</i> , 1998].	48
Figure 1.4 SiO _x films deposition using RF APPJ systems (a) Babayan <i>et al.</i> , 2001;(b) Nowling <i>et al.</i> ,2005; (c) Raballand <i>et al.</i> , 2009; (d) Yang <i>et al.</i> , 2009.....	49
Figure 2.1 Process flow chart.	50
Figure 2.2 Overview of the atmospheric pressure plasma jet system.	51
Figure 2.3 Processing of thin film deposition.	52
Figure 2.4 The schematic diagram of electrode configuration.	52
Figure 2.5 RF power supply.	53
Figure 2.6 Bubbler for liquid precursor.	53
Figure 2.7 HMDSO monomer structure and bond strengths.....	54
Figure 2.8 Optical emission spectroscopy.....	54
Figure 2.9 Scanning electron microscopy.....	55
Figure 2.10 Atomic force microscopy.	55
Figure 2.11 Fourier transform infrared (FTIR) spectroscopy.....	56
Figure 3.1 I-V-P curve of pure argon discharge (Ar flow rate: 5 slm).	57
Figure 3.2 I-V curves of Ar discharge with and without spring (Ar flow rate: 5 slm).	57
Figure 3.3 I-V curves of Ar, Ar+0.8% O ₂ , and Ar+4% O ₂ discharge (Ar flow rate: 5 slm)..	58
Figure 3.4 Breakdown voltage of the argon plasma mixed with various oxygen concentrations (Ar flow rate: 5 slm).	58
Figure 3.5 The electrical characteristics curves as a function of input power for different oxygen added into argon plasma (a) P- θ ; (b) P-Impedance; (c) P-Resistance; (d) P-Reactance (Ar flow rate: 5 slm).	59
Figure 3.6 Images for argon mixed with different concentrations of oxygen plasma and HMDSO introduced into downstream of discharge region (Ar flow rate: 5 slm; RF power: 50 W).	60
Figure 3.7 OES of argon mixed with different concentrations of oxygen plasma and HMDSO introduced into downstream of discharge region (Ar flow rate: 5 slm; RF power: 50 W).	61
Figure 3.8 OES of argon mixed with different concentrations of oxygen plasma and HMDSO introduced into downstream of discharge region at 180 to 400 nm (Ar flow rate: 5 slm; RF power: 50 W).	62
Figure 3.9 Species emitted of HMDSO dissociation (Ar flow rate: 5 slm; RF power: 50 W).	

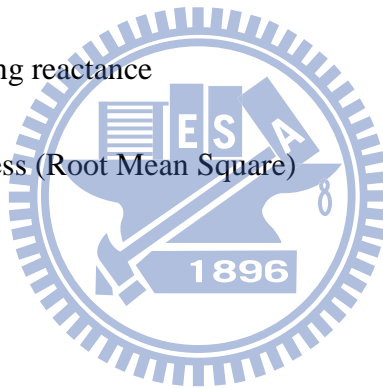
.....	62
Figure 3.10 OES of argon mixed with different concentrations of oxygen plasma and HMDSO introduced into downstream of discharge region at 400 to 700 nm (Ar flow rate: 5 slm; RF power: 50 W).	63
Figure 3.11 OES of argon mixed with different concentrations of oxygen plasma and HMDSO introduced into downstream of discharge region at 700 to 900 nm (Ar flow rate: 5 slm; RF power: 50 W).	64
Figure 3.12 SEM images of SiO _x thin film (a) cross section; (b) surface morphology on the 50 W RF power, 200 °C substrate temperature, 0 % oxygen concentration, 5 mm treatment distance and 200 passes.	65
Figure 3.13 AFM of SiO _x were deposited at different treatment passes (a) 4 passes; (b) 10 passes; (c) 20 passes; (d) 30 passes on the 50 W RF power, 200 °C substrate temperature, 0.8 % oxygen concentration, and 5 mm treatment distance.	65
Figure 3.14 Surface and cross section SEM of SiO _x showing thin films were deposited at different treatment passes (a) 4 passes; (b) 10 passes; (c) 20 passes; (d) 30 passes on the 50 W RF power, 200 °C substrate temperature, 0.8 % oxygen concentration, and 5 mm treatment distance.	66
Figure 3.15 Surface and cross section SEM of SiO _x showing thin films were deposited in different RF power (a) 35 W; (b) 40 W; (c) 50 W on 200 °C substrate temperature, 0.8 % oxygen concentration, 5 mm treatment distance and 20 passes.	67
Figure 3.16 Figure 3.6 Images for argon mixed with different concentrations of oxygen plasma and HMDSO introduced into downstream of discharge region (Ar flow rate: 5 slm; RF power: 50 W).	68
Figure 3.17 Surface SEM of SiO _x showing thin films were deposited at different treatment distance (a) 3 mm; (b) 5 mm; (c) 7.5 mm on 50 W RF power, 200 °C substrate temperature, 0.8 % oxygen concentration, and 20 passes.	68
Figure 3.18 Surface and cross section SEM of SiO _x showing thin films were deposited on the different substrate temperatures (a) 25 °C; (b) 100 °C; (c) 200 °C (d) 300 °C on 50 W RF power, 0.8 % oxygen concentration, 5 mm treatment distance and 60 passes.	69
Figure 3.19 Surface and cross section SEM of SiO _x showing thin films were deposited on the different substrate temperatures (a) 25 °C; (b) 100 °C; (c) 200 °C (d) 300 °C on 50 W RF power, 4 % oxygen concentration, 5 mm treatment distance and 20 passes.	70
.....	70
Figure 3.20 The schematic diagram of influence of substrate temperature.	71
Figure 3.21 Surface and cross section SEM of SiO _x showing thin films were deposited using argon plasma mixed with different oxygen concentrations (a) 0 %; (b) 0.2 %; (c) 0.8% (d) 2 %; (e) 4 %; (f) 10 % on 50 W RF power, 300 °C substrate temperature 5 mm treatment distance and 60 passes.	72

Figure 3.22 Deposition rate of SiO _x thin films deposited on the 200 and 300 °C substrate temperature as a function of oxygen concentration in the discharge.....	73
Figure 3.23 IR spectra of SiO _x thin films grown at substrate temperature 200 °C using argon plasma mixed with different oxygen concentrations (a) 1400-700 cm ⁻¹ ; (b) 4000-2400 cm ⁻¹	74
Figure 3.24 IR spectra of SiO _x thin films grown at substrate temperature 300 °C using argon plasma mixed with different oxygen concentrations (a) 1400-700 cm ⁻¹ ; (b) 4000-2400 cm ⁻¹	75
Figure 3.25 The ratio of shoulder area to mean peak area as a function of various oxygen concentrations mixed to argon plasma on the different substrate temperature.....	76
Figure 3.26 Evolution of oxygen to silicon ratio and carbon concentration of SiO _x thin films deposited at substrate temperature 200 °C using argon plasma mixed with different oxygen concentrations (passes: 20).....	77
Figure 3.27 Evolution of oxygen to silicon ratio and carbon concentration of SiO _x thin films deposited at different substrate temperature (oxygen concentration: 4 %; passes: 20).....	78
Figure 3.28 Image of super-hydrophobic surface.....	79
Figure 3.29 Change in the contact angle with the surface roughness (50W, 300 °C substrate temperature, 5 mm treatment distance and 60 treatment passes).	79



Nomenclature

P	RF input power
V	Measuring voltage
I	Measuring current
θ	Measuring phase angel between voltage and current
Z	Measuring impedance
R	Measuring resistance
X	Measuring reactance
Rq	Roughness (Root Mean Square)



Chapter 1 Introduction

1.1 Motivation

The technology of thin film deposition has been a rapid growth into the major research area for many years. Thin films have a number of applications in microelectronics, optics and nanotechnology. Scratch-resistance films, e.g. SiO_2 , are used to protect plastic materials and are also used as interlayers in semiconductor technology [Nowling *et al.*, 2005]. Most of the thin-film manufacturing processes have been fabricated by a number of methods, such as sputtering, plasma enhanced chemical vapor deposition (PECVD) and low-pressure chemical vapor deposition (LPCVD), among others [Plummer *et al.*, 2000]. Among these techniques, PECVD has demonstrated its superiority since the advantages of plasmas in materials processing include high deposition rate and uniform glow discharge which provide the uniform processing for a very large surface. However, the conventional PECVD process is expensive due to the requirement of costly vacuum equipment and frequent maintenance [Sawada *et al.*, 1995; Pai *et al.*, 1990].

In this study, we will focus on the development of a self-designed plasma jet system operating at the atmospheric pressure and used for deposition technology. The coaxial APPJ is driven by 13.56 kHz RF power in the process of depositing silicon oxide (SiO_x) film on silicon substrate. SiO_x films can be employed for a lot of applications in different fields such

as anti-scratch coating [Nowling *et al.*, 2005], low-k dielectric layers for microelectronic applications, as well as corrosion protective [Barchiche *et al.*, 2009] and super-hydrophobic coating [Yang *et al.*, 2009; Young *et al.*, 2008].

Most of the RF-APPJs were generated by using a mixture of helium and oxygen in SiO_x deposition, instead of the argon usually used. The major reason is that only an oxygen trace (ca 0.01%) can easily extinguish the plasma without a proper strategy. However, a stable, arc-free APPJ was produced with a spiral powered electrode covered by a quartz tube; this makes the addition of oxygen (up to 10%) possible without extinguishing the discharge in our study. In addition, argon is much cheaper than helium, and argon plasma provides better energy transfer efficiency than helium plasma [Wang *et al.*, 2003; Kasih *et al.*, 2007]. Therefore, we will focus that SiO_x deposition using argon mixed with oxygen RF-APPJ.

1.2 Background

1.2.1 Deposition of Silicon Oxide (SiO_x) Films and Its Applications

LPCVD (Low-Pressure Chemical Vapor Deposition), APCVD (Atmospheric-Pressure Vapor Deposition), and PECVD (Plasma Enhanced Chemical Vapor Deposition) have been investigated for many years for the deposition of silicon oxide (SiO_x, 1<x<2) thin films [Fujino *et al.*, 1990; Tochitani *et al.*, 1993; Plummer *et al.*, 2000]. SiO_x has been used for

passivation and insulation films in semiconductor devices and electronic parts. The process of SiO_x deposition is caused by thermal decomposition of the reaction monomer (silane or TEOS) in LPCVD and APCVD. The operating pressure of LPCVD is controlled in the range of 1 to 10 Torr and deposition temperature ranges from 400 to 800°C. The deposition temperature of APCVD is controlled in the range of 400 to 700°C.

Plasma enhanced chemical vapor deposition (PECVD) technology, conventionally operating at low pressure, has been investigated in the semiconductor-electronic and optical industries since the 80's. The mechanism of thin film deposition by PECVD is shown in Figure 1.1. The gas molecules are excited, ionized, or dissociated primarily in the plasma by electron impact. Then these excited molecules, atoms, radicals, and ions are transported and reach the substrate by diffusion under low-pressure condition. The particles reach the substrate surface, and further migrate and also find adsorption sites. Finally, the active molecular react with each other, resulting in film deposition [Konuma, 2005].

The conventional PECVD, using microwave, RF, and ECR discharges to deposit SiO_x films. Various silicon-containing precursors have been oxidized, such as silane (SiH_4) with N_2O , O_2 , or H_2O . The schematic of the system configuration for an LP-PECVD reactor is shown in Figure 1.2 [Pai *et al.*, 1990]. Other examples of common silicon-containing precursors used for LP-PECVD include TEOS ($\text{Si}(\text{OC}_3\text{H}_5)_4$), SiCl_4 , SiF_4 and HMDSN ($(\text{CH}_3)_3\text{SiNHSi}(\text{CH}_3)_3$). The deposition rate can be controlled from 0.1 to 2 nm/s and the

temperature of the substrate operated in the range of 100 to 400°C. The deposition system operated under reduced pressures, between 1.0 and 5000 mTorr [Konuma, 2005]. It is common that inorganic precursors used deposit SiO₂ film of LP-PECVD, such as silane (SiH₄). However, silane is toxic and easily ignited when exposed to air.

1.2.2 Classification of Atmospheric-Pressure Discharges

Atmospheric-pressure plasma has been shown as a great potential tool for thin film deposition because of its low cost, low temperature and possible continuous in-line process. Plasmas are subdivided into low temperature (LTP) and high temperature (HTP) plasmas and a further subdivision relates to thermal (thermal equilibrium) and non-thermal plasmas (see Table 1) [Hippler *et al.*, 2008]. Since we are interested in applying gas discharges (non-thermal plasma) under atmospheric-pressure condition, we further classify the atmospheric-pressure gas discharges. The various types of atmospheric pressure plasma [Schütze *et al.*, 1998] include, but not limit to, transferred arc and plasma torch, corona discharge, dielectric barrier discharge, and atmospheric-pressure plasma jet, as shown schematically in Figure. 1.3. They are briefly introduced in the following turn.

(a) Plasma Torch

The high gas temperature (3000-20000 K) operated using plasma torch (Figure 1.3 (a)). The plasma torch is the same as plasmas arc, and the advantage of these are high dissociation of

gas molecular and usually in the thin film coating. The above are also often called thermal plasmas and are in thermal equilibrium. However, it is not suitable for treating heat sensitive materials because the gas temperature is too high.

(b) Corona Discharge

In the corona discharge (Figure. 1.3 (b)), plasmas are generated around the tip of a needle, where the electric field is very large and non-uniform.

(c) Dielectric barrier discharge (DBD)

Figure 1.3 (c) which consists of two electrodes with at least one is coated with dielectrics. The discharge is maintained through a series of microdischarges. There are two major drawbacks for the corona discharge and the dielectric barrier discharge. One is the high breakdown voltage (5-25 KV) and the other is the difficulty of maintaining a uniform glow like low-pressure plasma. Since the plasmas are not uniform, it is limited for the cases where surface need to not smooth in deposition or etching.

(d) Plasma Jet

In plasma jet (Figure. 1.3 (d)), it often consists of two coaxial electrodes through which a mixture of gases flow. By applying 13.56 MHz RF power to the central electrode at a voltage in the range of several hundred volts, the gas discharge can be ignited and maintained over a fairly large range of conditions. Normally the atmospheric-pressure plasma jet is operated in the “abnormal glow” regime, in which the voltage increases with increasing current, while the

low-pressure plasma is often operated in the “normal glow” regime, in which the voltage remains constant with increasing current [Schütze *et al.*, 1998].

Schütze *et al.* summarized the range of breakdown voltages, plasma densities and oxygen related species densities of different plasma sources as shown in Table 2 and Table 3. It is clear that RF plasma jet can achieve stable discharge with much lower breakdown voltage (50-200 V) and appreciable plasma density (10^{11} - 10^{12} cm⁻³) in the discharge region. The densities of oxygen related species generated from plasma jet (e.g., 10^{16} cm⁻³ for both oxygen atoms and ozone) are not the best among these plasmas, but higher density of oxygen atom (10^{16} cm⁻³) that be well suited for the PECVD of SiO_x using RF-APPJ [Babayan *et al.*, 2001]. Another important advantage of the atmospheric-pressure plasma jet is that precursors for the thin film deposition can be introduced to the downstream of the discharge, which provides more flexibility of controlling the processing that cannot be achieved in low-pressure plasmas.

1.3 Literature Review

1.3.1 Deposition of SiO_x Films at Atmospheric-Pressure Condition

SiO_x can be deposited using an APPJ have been considered, such as microwave discharge [Pfuch *et al.*, 2003], DBD [Morent *et al.*, 2009; Bour *et al.*, 2008]. The operating

frequency of microwave discharge is much higher (2.54 GHz) than other discharges. There has not been very much to use of microwave discharge for thin film deposition, because the gas temperature is too high and it is not easy to design the equipment for thin film deposition [Alexandrov *et al.*, 2005]. The DBD has been widely studied for thin film deposition, however, the substrate was usually placed on between electrodes in the deposition process. It can be categorized into “direct AP-PECVD”, often leads to a number of complications and problems. The substrate placed on one of the electrodes and then a mixture of reactant gases introduced directly into the plasma region. It is easily caused complex reactions and result in the production of many reacting species which is unpredictable. Meanwhile, the damage of film is produced by bombardment of electrons and ions [Alexandrov *et al.*, 2005]. In contrast, the thin film deposition using RF-APPJ has been used for “remote AP-PECVD”, the deposition region is in the post discharge region, which can reduce the bombardment on the films. In addition, the remote PECVD can generally allow more independent parameter control than the direct PECVD, which may lead to better film quality. Since we are interested in developing thin films deposited in the remote region at atmospheric-pressure, and all the following literature surveys are restricted along this line.

The APPJ was generated by using the mixture of helium and oxygen between two coaxial metal electrodes that were driven by 13.56 MHz RF power supply [Babayan *et al.*, 2001], as shown in Figure 1.4 (a). The plasma exiting from between mixed with TEOS, and

directed onto a silicon substrate kept at 115 to 350 °C. The deposition rate was discussed with experimental parameters, such as substrate temperature, TEOS partial pressure, oxygen concentration, and RF power. Later, five precursors were examined including HMDSN, HMDSO, TMDSO, TMCTS and TEOS by using helium mixed with 2% oxygen plasma and the APPJ was driven by RF 27.12 MHz, as shown in Figure 1.4 (b). The results reported that high quality films without visible defects, such as cracking or chalkiness, could be obtained with precursors at specific deposition rates. However, the material exhibits poor abrasion resistance using TMDSO. They also found that coating, close to silicon dioxide (SiO₂) structure, with minimal OH and CH_x impurities; provide superior hardness and abrasion resistance [Nowling *et al.*, 2005].

As mentioned earlier, most of the RF-APPJs were generated by using the mixture of helium and oxygen. Helium and argon are used as the discharge gas in the RF-APPJ system. The other interesting thing is that, as oxygen is directly added into plasma, only helium is used, except the work done by [Ha *et al.*, 1995]. The major reason is that only trace of oxygen (ca 0.01 %) can easily extinguish the plasma with proper strategy. In addition, argon is much cheaper than helium, and argon plasma provides better energy transfer efficiency than helium plasma under the same working condition [Wang *et al.*, 2003; Kasih *et al.*, 2007]. Argon RF-APPJ system has been recently applied to deposit the SiO_x film without oxygen contained in the plasma region as shown in Figure 1.4 (c) and (d) [Yang *et al.*, 2009; Raballand V., *et al.*,

2009]. Rather, the oxygen is mixed with the precursor at the downstream of the APPJ. The thin film deposition rate increases significantly with oxygen flow rate; however, too much oxygen caused deposition rate decrease slightly since oxygen is an electronegative gas which could cause electron energy loss [Park et al., 2001]. Finally, Table 4 is shown as summary of important features for the SiO_x film deposited using APPJ at remote region. It is interesting and important to understand the influence of the oxygen addition on the SiO_x film deposition.

1.4 Specific Objectives and Organization of the Thesis

For this study, the fundamental characteristic of APPJ discharge and its application in the SiO_x deposited were investigated. The specific objectives of the present thesis can be summarized as followed:

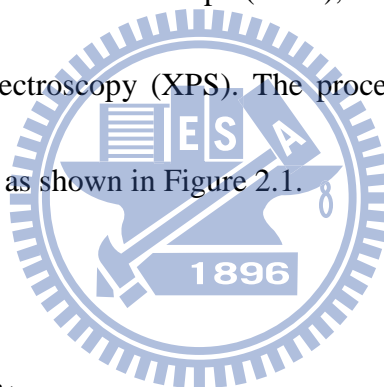
1. To diagnose the discharge characteristics of argon and argon mixed with oxygen (up to 10 %), including electrical and optical properties.
2. To deposit SiO_x films on the substrate using RF-APPJ in a stable, arc-free discharge.
3. To compare distinct operational factors to discuss the properties of thin film, including treatment passes, RF input powers, distances, substrate temperatures, and oxygen concentrations.
4. To measure SiO_x films properties using a Fourier transform infrared spectrometer (FTIR), an atomic force microscope (AFM), a scanning electron microscope (SEM),

the drop shape method for contact angle measurement instruments, and an X-ray photo electron spectrometer (XPS) under various testing conditions.



Chapter 2 Experimental Methods

In this study, we have designed and constructed the system for SiO_x film deposition using RF-APPJ. Plasma diagnostic measured, including electrically (IV characteristics, impedance analysis), optically (OES) and plasma temperature. For thin film deposition, the SiO_x films were deposited on P-type silicon substrates which were cleaned first. With distinct experimental factors, the properties of SiO_x films were analyzed by Fourier-transform infrared spectrometer (FTIR), atomic force microscope (AFM), scanning electron microscope (SEM), and X-ray photoelectron spectroscopy (XPS). The process flow chart of RF-APPJ system used for thin film deposition as shown in Figure 2.1.

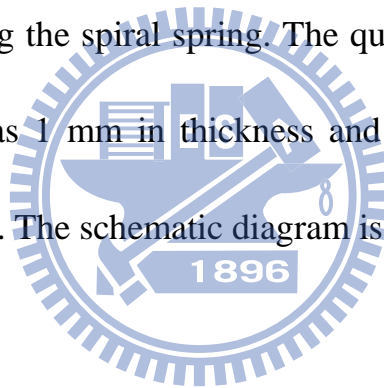


2.1 Experimental Facility

A schematic of the experimental setup of the proposed APPJ system driven by a 13.56 MHz RF power supply is shown in Figure 2.2. The experimental facility included 4 parts, RF power supply, matching and lines, gas feeding system, and electrode assembly. And the process of thin films deposition is shown in Figure 2.3.

2.1.1 APPJ System

A steel spring with a diameter of 4 mm was inserted between the stainless steel tube (outer diameter 3.2 mm) and a quartz tube (inner diameter 4 mm). Note the spring was in direct contact with the stainless steel tube, which both together was used as the power electrode. An aluminum tube with an inner diameter of 6 mm and 20 mm in length was placed outside the quartz tube and used as the ground electrode. The discharge gas (argon or argon mixed with oxygen) was passed through the space between the inner and outer electrodes following the spiral spring. The quartz tube extruding 5 mm from the end of electrodes was 1 mm in thickness and was used as the dielectrics to prevent the arc formation. The schematic diagram is shown in Figure 2.4.



2.1.2 RF Power Supply

The RF power was provided by a Dressler (model CESAR 1310) is shown in Figure 2.5. The frequency is 13.56 MHz, max output power is 1000 W into a 50 Ω load; it is connected to the APPJ through a matching box. Basic discharge parameters, such as the input RF power, RF voltage, RF current and phase angle, are measured by an RF impedance analyzer (MKS VI-probe-4100).

2.1.3 Matching Box

Matching Box used L-network the match way (RG-213/U) to make the connection after 50 Ω coaxial cable line effectively transmits the RF Power Generator electromagnetic wave to the APPJ chamber.

2.1.4 Gas Feeding System

The argon and oxygen gas (1/4 in the Teflon tube) connected the flow meters from the high-purity high-pressured steel cylinder. The flow rates of different gases were controlled by manually adjustable flow meter. The discharge gases, argon mixing with oxygen were fed into the gap between two electrodes to generate plasma. In this study, the flow rate of argon kept at 5 slm and mixed with various oxygen flow rates in the range of 0 to 0.5 slm (0 to 10 vol. %).

The organic silicon-containing precursor, HMDSO (Hexamethyldisiloxane, purchased from ACROS Organics, Germany, at 98% purity), is liquid phase and high vapor pressure at the room temperature. The properties of HMDSO are shown in the Table 5. The carrier gas, argon, flow rate was kept at 0.1 slm and fed into the bubbler which contain HMDSO liquid (Figure 2.6), and carrier gas and reactant vapor of monomer were delivered into post-discharge region. The monomer gas flow rate was kept at 4 g/h. The monomer structure and bond strengths are shown in Figure 2.7.

2.2 Experimental Instrumentation

The plasma generated using RF 13.56 power supply at atmospheric pressure, and the experimental instrumentation used to measure the properties of plasma such as V-I probe and oscilloscope for observation the plasma electrical. The species formations of plasma were detected by optical emission spectroscopy in the range of 180 to 900 nm. In the other hand, the film's thickness was measured by scanning electron microscope. The understanding of functional groups of SiO_x films were analyzed by Fourier transform infrared spectroscopy. Atomic force microscope used for measuring the surface roughness and observing the film's morphology. The surface chemical compositions were analyzed using X-ray photoelectron spectroscopy. The hydrophobic property of the SiO_x film's surface were measured using a contact angle machine, and the hardness was determined using the pencil test. Table 6 summarizes various instruments which were used for the measurements.

2.2.1 V-I Probe for Electrical Property Measurements

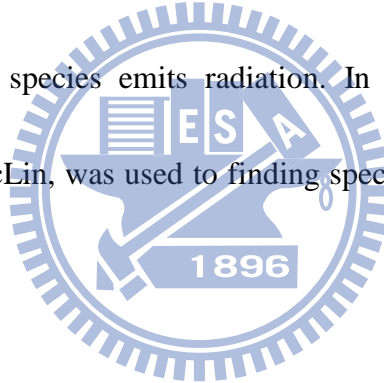
The V-I probe was provided by a MKS (model V-I probe 4100). V-I probe was one kind of RF Impedance Analyzers. The basic discharge parameters, such as RF voltage, RF current and phase angle were measured, and then by the computer, pushing back the impedance, delivered power, forward power, reflected power. V-I probe of the measurement and analysis

provided a best of a very useful tool, can also avoid some unnecessary depletion of power.

2.2.2 OES (Optical Emission Spectroscopy) for Species Identification

Measurements

The spectral optical emission intensities of RF-APPJ were measured using a monochromator (PI Acton SP 2500) with a photomultiplier tube (Hamamatsu R928) which was mounted on a mobile 3-D table (see Figure 2.8). The spectral range was 180-900 nm with 120 g/mm grating (Holographic, 300 nm Blaze and 500 nm Blaze). OES measuring is identifying which particles species emits radiation. In addition, a spectroscopy software package, named Plusus SpecLin, was used to finding specific lines in the spectra and excited species level change.



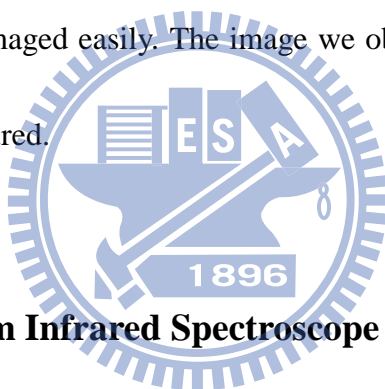
2.2.3 Scanning Electron Microscope (SEM) for Cross-section Morphology

Observation of Thin Film

The surface and cross-section morphology observed using scanning electron microscope (Hitachi S-4700I) is shown in Figure 2.9. SiO_x images by scanning it with a high-energy beam of electrons and producing signal of secondary electron that contains information about the film's surface morphology.

2.2.4 Atomic Force Microscope (AFM) for Surface Topology Observation

The AFM images were obtained in Veeco Dimension 5000 Scanning Probe Microscope (Figure 2.10), which consisted of a micro-scale cantilever with a sharp tip (probe) at its end that is used to scan the SiO_x film's surface. The cantilever was typically silicon or silicon nitride with a tip, and the tapping mode was used. The tip is not in contact directly with the surface and tip oscillated frequently when moved toward the surface until it begins to lightly touch. The tapping mode provides the resolution of 1 to 5 nm, it is lower than contact mode but the surface does not damaged easily. The image we obtained could 2D, 3D, and also the roughness data can be measured.



2.2.5 Fourier Transform Infrared Spectroscopy (FTIR) for Surface Bonding Identification

Fourier transform infrared (FTIR) spectroscopy is a measurement technique for collecting infrared spectra when vibration and rotating of molecule absorbed or transmitted infrared radiation. In this study, we analyzed the chemical structure and composition of SiO_x film with Perkin Elmer RX1 (Figure 2.11), scan range is from 4000 to 400 cm⁻¹ with resolution of 4 cm⁻¹ and each spectrum was obtained from an average of 32 scans.

2.2.6 X-ray Photoelectron Spectroscopy (XPS) for Surface Element Analysis

and Bonding Identification

X-ray Photoelectron spectroscopy (XPS) is a surface characterization spectroscopy. It is a spectroscopic technique to identify the elemental composition, and also measures empirical formula, chemical state and electronic state of the film's surface. We analyzed the surface element and compound with Ulvac-PHI 1600 (Mg anode at 250W and 15KV, 1253.6 eV, the electron take-off angle respect to the SiO_x film surface was 45°, chamber pressure below 2× 10⁻⁸ Torr).

2.2.7 Contact Angle Measurement Device

The surface of thin film was measured by contact angle measuring device using commercial KRUSS Easy Drop optical system (KRUSS GmbH-Germany). Distilled water drops of 10 μl were used as test liquid in our study. The values of the static contact angle obtained from Laplace-Young curve fitting based on the imaged sessile water drop profile.

2.2.8 Pencil Hardness Test

The hardness of SiO_x was determined using the pencil test (B-3084T). It have consists of 14 pencils, ranging in hardness from 6H to 6B. The hardest is a 6H, followed by 5H, 4H, 3H, 2H, H, F, HB, B, 2B, 3B, 4B, 5B, and 6B. The vertical force of 500 g is applied 45° is moved

over the deposited specimen. The one grade pencil be selected to start with scratching the surface, then test down the pencil grades until the first pencil that does not scratch the coating.

2.3 Experimental Procedures and Test Conditions

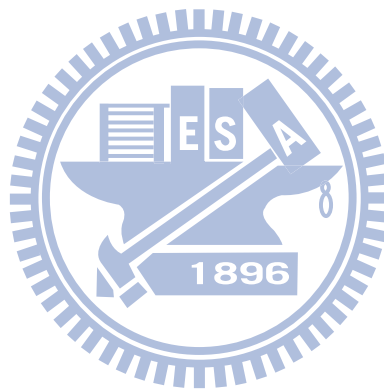
The self-designed APPJ system is shown in Figure 2.2. The plasma was generated between the electrodes using an RF 13.56 (MHz) power supply. The plasma diagnostics used included electrical (IV characteristics, impedance analysis), optical (OES) and gas temperatures. Testing conditions for the former confirmed the stability of plasma.

In this study, we used a P-type silicon wafer for use in the substrate for depositing SiO_x films. The procedures for sample preparation are shown as follows:

- (a) Cut wafer to 10 × 20 mm² and place in ultrasonic cleaner in acetone for 10 min.
- (b) Wash the sample with de-ionized water
- (c) Ultrasonic clean in ethyl alcohol for 10 min
- (d) Wash the sample with de-ionized water
- (e) Dry the sample with nitrogen gas

The precursor was fed into the downstream post-discharge, and reacted with plasma. Then, the silicon substrates were placed on the heating plate which moved back and forth by a moving stage, passed through the plasma jet and thin films deposited on the substrates. With distinct experimental factors, the properties of SiO_x films shall be analyzed.

The flow rate of the discharge gas was kept at 5 slm (18.3 m/s) for all conditions and the flow rate of carrier gas for HMDSO was kept at 0.1 slm (0.8 m/s). SiO_x films were deposited at various testing conditions, including treatment passes, RF input powers (35-50 W), distances (3-7.5 mm), substrate temperatures (room temperature - 300°C), and oxygen concentrations (0-10 %). All of the samples deposited on the moving stage were fixed at 10 mm/s. Argon mixed with various oxygen concentrations (0 to 10%). The testing condition of RF-APPJ for SiO_x deposition has been summarized in Table 7.



Chapter 3 Results and Discussion

3.1 Electrical Characterization of the APPJ System

An APPJ, using RF power, has been developed to produce a homogeneous glow, and discharge parameters have been discussed [Li *et al.*, 2006].

$$\text{The impedance: } Z = \frac{V}{I} \quad (3-1)$$

$$\text{The resistance: } R = \left(\frac{V}{I}\right) \cos \theta \quad (3-2)$$

$$\text{The reactance: } X = \left(\frac{V}{I}\right) \sin \theta \quad (3-3)$$

$$\text{The phase angle: } \frac{X}{R} \quad (3-4)$$

The discharge characteristics of APPJ can be discussed by relationships among I_{rms} , V_{rms} , power, impedance, and phase angle. A typical I-V discharge characteristic of pure argon at a 5 slm flow rate is shown in Figure 3.1. Input power was controlled in the range of 0 to 60W, and dark discharge occurred before the voltage breakdown of 580 V. After voltage breakdown, the current and voltage increased linearly (abnormal discharge) and plasma was generated. In addition, Figure 3.2 illustrates voltage and input power for pure argon plasma, with and without spring as a function of current, respectively. Without the use of a spiral electrode, the breakdown voltage was as high as 718 V. After the breakdown process, the voltage drop to 433 V and then increased with the rising current. A stable discharge was observed as compared to the case without a spiral electrode under the same power input. Because a strong

electrical field occurred at the smaller electrode gap when using a spiral electrode, results showed a decrease in breakdown voltage. Figure 3.3 illustrates voltage for argon mixed with various oxygen concentrations in plasma as a function of current. The electrical properties of argon mixed with oxygen, discharged with the use of a spiral electrode, were similar to pure argon discharge. Only the breakdown voltage increased because an electronegative gas, such as oxygen, was added to the plasma [Park *et al.*, 2001]. The measured minimum voltage required to sustain the argon mixed with oxygen plasma, which would be increased by increasing the oxygen concentration, are shown in Figure 3.4. The relationship between input power and the other electrical properties, such as phase angle, impedance, resistance, and reactance, are shown in Figure 3.5. Before plasma is generated, the coaxial electrode is like a pure capacitive and the current led the voltage nearly 90° in phase. When input power was increased continuously, the phase angle decreased slightly in the range of 1° (Figure 3.5 (a)). It is different than the greater phase shift of a current leading the voltage of pure argon or that mixed with oxygen plasma using RF-APPJ because of the inner quartz tube between the power and grounded electrode [Wang *et al.*, 2003]. The impedance decreased with input power and increased with oxygen added (Figure 3.5 (b)). The impedance is combined with resistance and reactance terms [Zhu *et al.*, 2005], resistance increased in the range of 2 to 3 Ω but the decrease in reactance was in the range of 3 to 8 Ω with input power (Figure 5 (c) and (d)). Therefore, the impedance trend was to decrease with the decrease in reactance.

3.2 Visual Observation and Optical Emission Spectral Analysis of APPJ

Typical images for argon mixed with plasma of different oxygen concentrations and HMDSO was fed into the downstream of the discharge are shown in Figure 3.6. For pure argon discharge, the plasma plume gave an emission of violet light. When HMDSO was fed into the downstream of the discharge region, the color of the plasma plume changed to blue. The color of the plasma plume appears to darken slowly when oxygen was fed into the plasma. The changes in the color of the plasma can be explained clearly by OES measurement and relative optical emission shown in the range of 180 to 900 nm in Figure 3.7. Then the OES was analyzed by dividing it into three spectral ranges, 180 to 400 nm, 400 to 700 nm, and 700 to 900 nm to compare pure argon, argon mixed with oxygen, and HMDSO that was introduced downstream of the discharge. The OES reveals the presence of excited fragments of the monomer structure $((\text{CH}_3)_3\text{-Si-O-Si-(CH}_3)_3)$, such as Si, Si-O, CH, and C2 [Granier *et al.*, 2002; Wang *et al.*, 2005; Chen *et al.*, 2006]. The Si-C and C-H in the monomer are easily broken by an electron or a high energy metastable radical, since the bond energy of Si-C (4.6 eV) and C-H (3.5 eV) is lower than Si-O (8.3 eV). Excited Si atom emission was evident from the argon plasma and HMDSO introduced downstream of the discharge, and there was a relative line decay when oxygen was fed into the plasma, as shown in Figure 3.8. The excited Si atom was emitted in the UV region from Si-O-Si broken from the monomer because pure

argon easily generates more electrons of higher energy radicals than oxygen added into plasma. Due to the fact that oxygen is characteristic of an electronegative, electrons generated from plasma easily decrease. This phenomenon is likely to decrease the ability of a monomer to be polymerized. Similarly, the detected line of Si-O fragments at 216 to 290 nm is shown in Figure 3.9. The spectral, ranging from 400 to 700 nm, presents carbon-containing species (CH, C₂) detected from argon plasma and HMDSO introduced downstream of the discharge, and the relative emission appeared in the emission of a blue light region of 400 to 500 nm (Figure 3.10). In addition, the region of 700 to 800 nm was detected from excited Ar atom emission (Figure 3.11). Pure argon discharge exhibited the highest intensity of the other test cases. When oxygen was fed into plasma or HMDSO was introduced downstream of the discharge, the emission intensity of the argon region decreased, partially due to the energy needed to dissociate or ionize the oxygen and HMDSO molecules.

3.3 Surface Morphology and Deposition Rate of Thin Film

The surface morphology of SiO_x films was observed using SEM, and the thickness of the films was measured from the SEM cross section images. Thin films were deposited on the substrate using a moving stage controlled at 10 mm/s per pass and an inner diameter tube of 4 mm. The residence time of one pass is 0.4 s. Figures 3.12 (a) and (b) show SEM cross section images and surface morphology of the SiO_x film, respectively. In this case, the total residence

time was 80 s for 200 passes and the thickness of the thin film was 120 nm. Thus, the deposition rate was 90 nm/min. The roughness of the thin films measured by AFM and the scan size of the samples was $2 \times 2 \mu\text{m}$. In addition, the plasma temperature of 100°C was measured at 5 mm from the exit of the quartz tube using a K type thermocouple.

3.3.1 Effect of Number of Treatment Passes

The surface morphology of SiO_x thin films observed under various treatment passes are shown in Figure 3.13. The morphology of the surface structure changed from 4 passes to 30 passes. The beginning of thin film grown on the surface can be found via 4 passes and the surface roughness was 2.2 nm (Figure 3.13 (a)). The thickness of the thin films measured about 100, 200, and 350 nm via 10, 20, and 30 treatment passes, respectively. SEM surface images are shown in Figure 3.14. The particle size and roughness of the thin films also increased with the increasing number of treatment passes.

3.3.2 Effect of Input Power

Figure 3.15 shows the effect of the RF power on the thickness of thin films from 35 W to 50 W. If the RF power was less than 35 W, the deposition rate of the thin film was too slow to be measured. The thickness of the thin films exhibits dependence on the RF power, and it

corresponds to the increase in the concentration of active species such as excited argon atoms or excited molecules of oxygen in the plasma stream from the discharge region [Alexandrov *et al*, 2005]. The concentration of argon metastable excited atoms increased with the increase of RF power and caused partial dissociation and formation of silicon-containing active species which further enhanced the deposition rate of thin films.

3.3.3 Effect of Treatment Distance

Figure 3.16 shows the effect of the thickness of thin films on various treatment distances ranging from 3 mm to 7.5mm (from the end of the quartz tube). The thickness of the thin films deposited exhibits a strong dependence on treatment distance. HMDSO monomer dissociated via plasma formed the silicon-containing active species and further polymerized on the surface. If the substrate was close to the exit of the monomer, the active species increased and the deposition rate was enhanced. Contrarily, the active species were easily quenched in the ambient via far distance treatment. However, the 3 mm treatment distance was not better for higher deposition rate where the thin film exhibited rough surfaces and loose structure of big particles, as shown in Figure 3.16 (a) and Figure 3.17 (a).

3.3.4 Effect of Substrate Temperature

The effect of various substrate temperatures heated in the range from room temperature to 300°C, and thin films deposited when 0.8% oxygen was added to the discharge are shown in Figure 3.18. Not thin film formation, but polymerization of the HMDSO at low substrate temperatures was found, as shown in Figures 3.18 (a) and (b). There was no solid-state structure of thin film formation and a grease surface presented on the substrate. Figure 3.19 (a) shows the same situation when argon is mixed with 4% oxygen and added into the discharge. In addition, it is interesting to compare the thickness of thin films at the various substrate temperatures.

The thickness of thin films deposited in the same treatment passes showed a strong negative dependence on the substrate temperature and many authors have discussed this situation using atmospheric pressure plasma [Babayan *et al.*, 2001; Huang *et al.*, 2009]. The sticking coefficient of the active molecule species formed from the plasma region decreased as substrate temperature increased. The ability of molecules to absorb the substrate reduced, but thermal diffusion of the molecules was enhanced at high substrate temperatures to diffuse into the suited sites of the thin film and caused dense film formation, the schematic diagram as shown in Figure 3.20.

3.3.5 Effect of Oxygen Concentration in the Discharge

The effect of film characteristics on deposition, using argon plasma mixed with various oxygen concentrations, is shown in Figure 3.21. The thickness and surface morphology of thin films deposited in the same treatment passes showed a strong positive dependence on oxygen concentration. The thickness of film deposited using pure argon plasma was hard to measure accurately. Thus the deposition rate was calculated to be 37.5 nm/min via increasing passes to 200. When oxygen added into argon plasma increased to 0.2 and 0.8%, the deposition rate was 200 and 275 nm/min, respectively. Surface roughness of deposited pure argon plasma was 1.38 nm. When oxygen introduced into argon plasma increased to 0.2 and 0.8%, the roughness was 5.26 and 29.8 nm, respectively. High mechanical strength with a smooth and transparent surface of SiO_x thin film can be formed using argon plasma mixed with oxygen below 0.8% at 300°C substrate temperature. However, oxygen addition was more than 2 %, particles of a hundred nanometer scale were observed and films lost their transparency, powdery structure formed (see Figure 3.21 (d) to (f)). The possible results of reaction between the silicon-containing species and oxygen, and further cause nucleation in gas phase [Kasih *et al.*, 2007].

Figure 3.22 shows the relationship between the deposition rate and oxygen concentration in the discharge at various substrate temperatures. Oxygen plays an important role in the low-pressure PECVD [Theil *et al.*, 1994] and atmospheric-pressure PECVD system [Sawada

et al., 1995; Zhu *et al.*, 2005] to SiO_x films. The oxygen radicals generated from argon mixed with oxygen at discharge, and excited oxygen promote decomposition of monomer molecules. Therefore, the deposition rate increases by adding oxygen.

Further hardness testing briefly is presented in Table 8 under variation conditions. For the 200 °C substrate temperature, the lowest deposition rate (90 nm/min) of pure argon plasma has a rating of 5H in thickness of 100 and 300 nm. However, the film exhibited a lower pencil hardness of HB if oxygen added to 0.8%. For the 300 °C substrate temperature, the deposition rate was decreased from 1200 nm/min to 275 nm/min and the hardness evidently raised to 4H.

3.4 Bond Structure Analysis by FTIR

The bond structure of SiO_x film was analyzed by Fourier Transform Infrared (FTIR) Spectroscopy. The resolution of 4 cm⁻¹ for all spectra and each spectrum was obtained from an average of 32 scans. SiO_x exhibits three characteristic absorption peaks at rocking (450 cm⁻¹), bending (800 cm⁻¹), and asymmetric stretching (1075 and 1150 cm⁻¹). An organic component of the absorption peak exhibits at 840 cm⁻¹ (Si-CH₃ stretching in the Si-(CH₃)₃ group) and 800 cm⁻¹ (Si-CH₃ stretching in the Si-(CH₃)₂ or the Si-(CH₃) group). The Si-CH₃ bending mode at 1273 cm⁻¹ and the CH₃ stretching mode at around 2960 cm⁻¹ can be observed. The broad absorption bands at around 3400 cm⁻¹ are attributed to OH bending and absorption at 940 cm⁻¹ is attributed to the Si-OH [Sawada *et al.*, 1995; Raballand *et al.*, 2009]. The bond structure of

the deposition films formed by adding various oxygen concentrations was analyzed by FTIR at 200 and 300°C as shown in Figure 3.23 and Figure 3.24, respectively. It can be seen that organic components (CH₃ or Si-CH₃ groups) changed with the addition of oxygen and are shown in Figure 3.23 (a) and Figure 3.24 (a). When oxygen gas is added into the plasma region, and atom oxygen radicals and excited oxygen molecules are generated, it can partially decompose the carbon-containing groups of HMDSO monomer in the gas-phase or substrate surface [Sawada *et al.*, 1995; Wavhal *et al.*, 2006]. Therefore, the absorption peaks related to thin film carbon were decreased by adding oxygen into the plasma.

Many authors who have discussed the degree of SiO_x thin film porosity use the ratio of shoulder area at 1150±10 cm⁻¹ to mean peak area at 1075±5 cm⁻¹ [Nowling *et al.*, 2005]. The relationship between degree of porosity and addition of oxygen is shown in Figure 3.25, and the trend is shown that the more oxygen that is added to the plasma, the higher the degree of porosity of film obtained. Meanwhile, higher substrate temperatures evidently decrease the porosity of the film. It can be interpreted as a higher deposition rate easily causes a higher degree of porosity. In addition, the OH group of films was measured at around 3400 cm⁻¹, as shown in Figure 3.23 (b) and Figure 3.24 (b), which attributed to OH bending during and after deposition, and following exposure to atmospheric vapor [Raballand *et al.*, 2009]. The peak, at 3400 cm⁻¹, increased absorption with the addition of oxygen at 200°C substrate temperature. This can be explained by little vapor inside the porosity of the film, but the broad absorption

on the substrate at a temperature of 300°C clearly disappeared.

3.5 Surface Composition Analysis by XPS

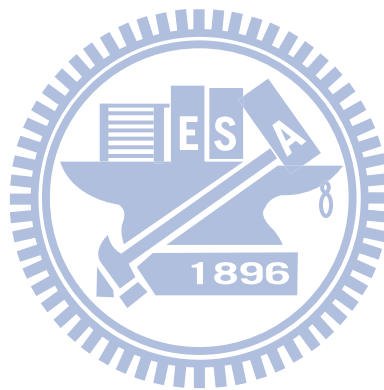
Surface composition was analyzed by x-ray photoelectron spectroscopy and the surface of each sample was cleaned by ion gun sputtering for 30 s. We compared the various oxygen concentrations added to the plasma to the effects of the oxygen-to-silicon ratio (O/Si) and carbon-to-oxygen ratio (C/O), as shown in Figure 3.26. It can be seen that the O/Si ratio increased with the increase of oxygen concentration. The O/Si ratio of the film deposited using pure argon plasma was low, 1.31. This may have been caused by a fraction of the monomer being formed from post discharge of pure argon plasma, and a decrease in polymerization reaction ability. C/O ratio groups do not reduce efficiently (18.3%) because there is not enough excited oxygen to promote decomposition of the monomer. Adding oxygen concentration increased O/Si ratio to 1.56 at 4% oxygen concentration but lowered slightly to 1.51 at 10% oxygen concentration. C/O ratio decreased with the increase of oxygen concentration. The element composition of thin films under various oxygen concentrations is shown in Table 9. In addition, the relationship between films deposited at various substrate temperatures, and O/Si ratio and C/O were also analyzed using 4% oxygen concentration added to plasma, as shown in Figure 3.27. At a lower substrate temperature, 25°C, thin film was not deposited but there was a polymerization reaction and an O/Si ratio of 1.26. Carbon

concentration evidently decreased from 23.8% to 10.5% when the substrate temperature increased from 25°C to 300°C. The element composition of thin films under various substrate temperatures is shown in Table 10. It could be because the thermal decomposition of the carbon-containing group at higher substrate temperatures [Huang *et al.*, 2009].

3.6 Contact Angle Measurements

SiO_x thin film is one material available for producing a hydrophobic and super-hydrophobic coating [Yang *et al.*, 2009; Ji *et al.*, 2009]. Its application includes self-cleaning and reduced contamination. A rough surface and low surface energy are important to enhance hydrophobicity of the surface. In our study, surface roughness changes can be accomplished by controlled distinct experimental parameters, including oxygen concentrations, substrate temperatures, and treatment passes. The SiO_x film with a low surface energy functional group (-CH₃), was measured by an FTIR instrument as shown in Figure 3.24 (a). The image of silicon substrate was treated and untreated as shown in Figure 3.28, the SiO_x with super-hydrophobic surface of right side. Figure 3.29 shows that the effect of the water contact angle of deposited films depends on controlling various oxygen concentrations being added into the discharge. When oxygen was added to 0.2%, the surface roughness of the film was 5.3 nm and the measurement of contact angle was 81.4°. A super-hydrophobic surface formed when oxygen was added to 0.8%, the contact angle measured was more than

150°, and the surface roughness was 29.7 nm. As the oxygen added to 2% (or more), although the measurement of contact angle was higher than 150°, the powdery structure was formed and probably limited its applicability.



Chapter 4 Concluding Remarks

4.1 Summary

The deposition of SiO_x films, from pure HMDSO, by means of argon mixed with oxygen atmospheric-pressure plasma jet was studied. SiO_x deposited under various test conditions, and properties of thin film have been discussed. Results show that various oxygen concentrations added into argon plasma and substrate temperature greatly affected the properties of SiO_x film. A higher deposition rate was obtained at higher oxygen concentrations, but more oxygen addition (2-10%) caused the highly porous structure formation, the particles of a hundred nanometer scale were observed. Meanwhile, the O/Si ratio increased with oxygen addition.

It was found that the various substrate temperatures controlled in the deposition process evidently affected the deposition rate, degree of porosity, and chemical composition of the SiO_x . Deposition rate decreased with increasing substrate temperature. Lower degree of porosity and less OH in the film was obtained under the higher substrate temperatures, and SiO_x provided the excellent hardness surface. Carbon atoms in the film decreased, it could be because the thermal decomposition of the carbon-containing group at higher substrate temperatures.

The surface roughness of SiO_x films can be controlled by various oxygen additions, and

films with the function group, $-CH_3$, which may enhance the hydrophobicity of the surface. A super-hydrophobic surface, water contact angle greater than 150° , formed when oxygen was added to 0.8% (or more).

4.2 Recommendations of Future Work

According to this study, the future work is suggested as following,

1. We expect to find the suited condition to deposit the super-hydrophobic surface of SiO_x films on the glass as well as high UV-VIS transmission;
2. To compare the silicon oxide using various precursors, such as HMDSN, TEOS;
3. To compare the characteristic of SiO_x films when oxygen be added in the post-discharge region with the carrier gas for precursor;
4. The refractive index and dielectric constant of SiO_x film shall be measured. And further, SiO_x films can be employed for a lot of applications in different fields such as corrosion protective coating;
5. We shall develop the planar RF-APPJ system for continuous in-line processing of large sheet.

References

- [1] Alexandrov S.E., McSparran N., and Hitchman M.L., "Remote AP-PECVD of silicon dioxide films from hexamethyldisiloxane (HMDSO)", Chemical Vapor Deposition, Vol. 11, Issue 11-12, pp. 481-490, 2005.
- [2] Babayan S.E., Jeong J.Y., Tu V.J., Park J., Selwyn G.S., and Hicks R.F., "Deposition of silicon dioxide films with an atmospheric-pressure plasma jet", Plasma Sources Science and Technology, Vol. 7, Issue 3, pp. 286-288, 1998.
- [3] Babayan S.E., Jeong J.Y., Schütze A., Tu V.J., Moravej M., Selwyn G.S., and Hicks R.F., "Deposition of silicon dioxide films with a non-equilibrium atmospheric-pressure plasma jet", Plasma Sources and Science Technology, Vol. 10, Issue 4, pp. 573-578, 2001.
- [4] Barchiche C.E., Rocca E. and Hazan J., "Corrosion behaviour of Sn-containing oxide layer on AZ91D alloy formed by plasma electrolytic oxidation", Surface and Coatings Technology, Vol. 2, Issue 17, pp. 4145-4152, 2009.
- [5] Benedikt J., Raballand V., Yanguas-Gil A., Focke K., and von Keudell A., "Thin film deposition by means of atmospheric pressure microplasma jet", Plasma Physics and Controlled Fusion, Vol. 49, Issue 12B, pp. B419-B427, 2007.
- [6] Bour J., Bardon J., Aubriet H., Frari D.D., Verheyde B., Dams R., Vangeneugden D., Ruch D., "Different ways to plasma-polymerize HMDSO in DBD configuration at

- atmospheric pressure for corrosion protection”, Plasma Processes and Polymers, Vol. 5, Issue 8, pp. 788-796, 2008.
- [7] Dowling D.P., Ramamoorthy A., Rahman M., Mooney D.A., and MacElroy J.M.D., “Influence of atmospheric plasma and gas composition on the properties of deposited siloxane coating”, Plasma Processes and Polymers, Vol. 6, pp. S483-S489, 2009.
- [8] Fujino K., Nishimoto Y., Tokumasu N., and Maeda K., “Silicon dioxide deposition by atmospheric pressure and low-temperature CVD using TEOS and ozone”, Solid-State Science and Technology, Vol. 137, Issue 9, pp. 2883-2887, 1990.
- [9] Granier A., Vervloet M., Aumaille K., and Vallee C., “Optical emission spectra of TEOS and HMDSO derived plasmas used for thin film deposition”, Plasma Sources Science and Technology, Vol. 12, Issue 1, pp. 89-96, 2003.
- [10] Ha H.K., Inomata K., and Koinuma H., “Plasma chemical vapor Deposition of SiO₂ on air-exposed surfaces by cold plasma torch”, Journal of the Electrochemical Society, Vol. 142, Issue 8, pp. 2726-2730, 1995.
- [11] Hippler R., Kersten H., Schmidt M., and Schoenbach K.H., Low Temperature Plasmas-Fundamentals, Technologies and Techniques, Vol. 2, 2nd, Wiley-VCH, 2008.
- [12] Huang C., Liu C.H., Su C.H., Hsu W.T., and Wu S.Y., “Investigation of atmospheric-pressure plasma deposited SiO_x films on polymeric substrates”, Thin Solid Films, Vol. 517, Issue 5141-5145, 2009.

- [13] Huang C., Liu C.H., Wu S.Y., “Surface characterization of the SiO_x films prepared by a remote atmospheric pressure plasma jet”, Surface and Interface Analysis, Vol. 41, Issue 1, pp. 44-48, 2009.
- [14] Ji Y.Y., Kim S.S., Kwon O.P., and Lee S.H., “Easy fabrication of large-size superhydrophobic surfaces by atmospheric pressure plasma polymerization with non-polar aromatic hydrocarbon in an in-line process”, Applied Surface Science, Vol. 255, Issue 8, pp. 4575-4578, 2009.
- [15] Kasih T.P., Kuroda S.I., and Kubota H., “A nonequilibrium, atmospheric-pressure argon plasma torch for deposition of thin silicon dioxide films”, Chemical Vapor Deposition, Vol. 13, Issue 4, pp. 169-175, 2007.
- [16] Konuma M., Film Deposition by Plasma Techniques, Springer-Verlag, Heidelberg, 1992
- [17] Li S.Z., Lim J.P., Kang J.G., and Uhm H.S., “Comparison of atmospheric-pressure helium and argon plasmas generated by capacitively coupled radio-frequency discharge”, Physics of Plasma, Vol. 13, Issue 9, 2006.
- [18] Matsuura M., Hayashide Y., Kotani H., and Abe H., “Film characteristics of APCVD oxide using organic silicon and ozone”, Japanese Journal of Applied Physics Part 1, Vol. 30, Issue 7, pp. 1530-1538, 1991.
- [19] Morent R., Geyter N.D., Jacobs T., Vlierberghe S.V., and Dubruel P., “Plasma-polymerization of HMDSO using an atmospheric pressure dielectric barrier

- discharge”, Plasma Processes and Polymers, Vol. 6, Issue S1, pp. S537-542, 2009.
- [20] Nowling G.R., Yajima M., Babayan S.E., Moravej M., Yang X., Hoffman W., and Hicks R.F., “Chamberless plasma deposition of glass coatings on plastic”, Plasma Sources Science Technology, Vol. 14, Issue 3, pp. 477-484, 2005.
- [21] Pai C.S., and Chang C.P., “Downstream microwave plasma-enhanced chemical vapor deposition of oxide using tetraethoxysilane”, Journal of Applied Physics, Vol. 68, Issue 793, pp.793-801, 1990.
- [22] Park. J, Henins I, Herrmann H.W., and Selwyn G.S., “Gas breakdown in an atmospheric pressure radio-frequency capacitive plasma source”, Journal of Applied Physics, Vol. 89, Issue 1, pp. 15-19, 2001.
- [23] Pfuch A., and Cihar R., “Deposition of SiO_x thin films by microwave induced plasma CVD at atmospheric pressure”, Surface and Coating Technology, Vol. 183, Issue 2-3, pp. 134-140, 2004.
- [24] Plummer J.D., Deal M.D., Griffin P.B., Silicon VLSI Technology Fundamentals, Practice and Modeling, Prentice Hall, NJ, 2000.
- [25] Raballand V., Benedikt J., Hoffmann S., Zimmermann M., and von Keudell A., “Deposition of silicon dioxide films using an atmospheric pressure microplasma jet”, Journal of Applied Physics, Vol. 105, Issue 8, 2009.
- [26] Sawada Y., Ogawa S., and Kogoma M., “Synthesis of plasma-polymerized

- tetraethoxysilane and hexamethyldisiloxane films prepared by atmospheric-pressure glow discharge”, Journal of Physics D: Applied Physics, Vol. 28, Issue 8, pp. 1661-1669, 1995.
- [27] Shakir S., Mynampati S., Pashaie B., and Dhali S.K., “rf-generated ambient-afterglow plasma”, Journal of Applied Physics, Vol. 99, Issue 7, 2006.
- [28] Schütze A., Jeong J.Y., Babayan S.E., Park J., Selwyn G.S., and Hicks R.F., “The atmospheric-pressure plasma jet: a review and comparison to other plasma sources”, IEEE Transactions on Plasma Science, Vol. 26, Issue 6, pp. 1685-1694, 1998.
- [29] Theil J.A., Brace J.G., and Knoll R.W., “Carbon content of silicon-oxide films deposited by room-temperature plasma-enhanced chemical-vapor-deposition of hexamethyldisiloxane and oxygen”, Journal of Vacuum Science and Technology A-Vacuum Surfaces and Films, Vol. 12, Issue 4, pp. 1365-1370, 1994.
- [30] Tochtani G., Shimosuma M., and Tagashira H., “Deposition of silicon oxide films from TEOS by low frequency plasma chemical vapor deposition”, Journal of Vacuum Science and Technology A-Vacuum Surfaces and Films, Vol. 11, Issue 2, pp. 400-405, 1993.
- [31] Wang S., Schulz-von der Gathen V., and Dobele H.F., “Discharge comparison of nonequilibrium atmospheric pressure Ar/O₂ and He/O₂ plasma jets”, Applied Physics Letters, Vol. 83, Issue 16, Issue 16, pp. 3272-3274, 2003.
- [32] Wang Y., Zhang J., and Shen X.Y., “Surface structures tailoring of hexamethyldisiloxane

- films by pulse rf plasma polymerization”, Materials Chemistry and Physics, Vol. 96, Issue 2-3, pp. 498-505, 2006.
- [33] Wavhal D.S., Zhang J., Steen M.L., and Fisher E.R., “Investigation of gas phase species and deposition of SiO₂ films from HMDSO/O₂ plasmas”, Plasma Processes and Polymers, Vol. 3, Issue 3, pp. 276-287.
- [34] Yang S.H., Liu C.H., Su C.H., and Chen H., “Atmospheric-pressure plasma deposition of SiO_x films for super-hydrophobic application ”, Thin Solid Films, Vol. 517, Issue 17, pp. 5274-5287, 2009.
- [35] Yoshiki H., Abe K., and Mitsui T., “SiO₂ thin film deposition on the inner surface of a poly (tera-fluoroethylene) narrow tube by atmospheric-pressure glow microplasma”, Thin Solid Films, Vol. 515, Issue 4, pp. 1394-1399, 2006.
- [36] Zhu W.C., Wang B.R., Yao Z.X. and Pu Y.K., “Discharge characteristics of an atmospheric pressure radio-frequency plasma jet”, Journal of Physics D: Applied Physics, Vol. 38, Issue 9, pp. 1396-1401, 2005.
- [37] Zhu X.D., Arefi-Khonsari F., Petit-Etienne C., and Tatoulian M., “Open air deposition of SiO₂ films by an atmospheric pressure line-shaped plasma”, Plasma Processes and Polymers, Vol. 2, Issue 5, pp. 407-413, 2005.

Table

Table 1 Subdivision of plasmas [Hippler *et al.*, 2008].

Low-temperature plasma (LTP)		High-temperature plasma (HTP)
Thermal LTP	Non-thermal LTP	
$T_e \approx T_i \approx T \leq 2 \times 10^4 \text{ K}$	$T_i \approx T \approx 300 \text{ K}$	
	$T_i \ll T_e \leq 10^5 \text{ K}$	$T_i \approx T_e \geq 10^7 \text{ K}$
e.g., arc plasma at normal pressure	e.g., low-pressure glow discharge	e.g., fusion plasmas

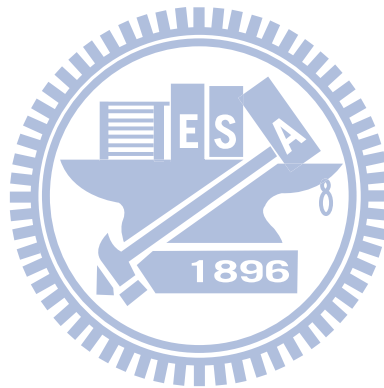


Table 2 Comparison of plasmas sources [Schutz *et al.*, 1998].

Source	Breakdown voltage (kV)	Plasma density (cm ⁻³)
Low-pressure discharge	0.2 – 0.8	10 ⁸ - 10 ¹³
Arc and plasma torch	10 – 50	10 ¹⁶ - 10 ¹⁹
Corona	10 – 50	10 ⁹ - 10 ¹³
Dielectric barrier discharge	5 – 25	10 ¹² - 10 ¹⁵
Plasma jet	0.05 – 0.2	10 ¹¹ - 10 ¹²

Table 3 Density of oxygen species in the plasma discharge [Schutz *et al.*, 1998].

Source	Density (cm ⁻³)		
	O ⁺ , O ₂ ⁺ , O ⁻	O	O ₃
Low-pressure discharge	10 ¹⁰	10 ¹⁴	< 10 ¹⁰
Arc and plasma torch	10 ¹⁵	10 ¹⁸	< 10 ¹⁰
Corona	10 ¹⁰	10 ¹²	10 ¹⁸
Dielectric barrier discharge	10 ¹⁰	10 ¹²	10 ¹⁸
Plasma jet	10 ¹²	10 ¹⁶	10 ¹⁶

Table 4 Summary of important features for SiO_x thin films deposition using APPJ at remote region.

Authors	Discharge gas	Precursor	Carrier gas	Sub. Temp.	Electrode	Power	Deposition rate
Babayan <i>et al.</i> , 2001	He (757 torr) + O ₂ (3 torr)	TEOS (7 mtorr)	He	115~350	RF-APPJ	280 W	25~70 nm/min
Babayan <i>et al.</i> , 1998	He(757 torr) + O ₂ (3 torr)	TEOS (0.2 torr)	He	115~350	RF-APPJ	400 W	300 nm/min
Benedikt <i>et al.</i> , 2007	Ar (3 slm)	HMDSO (0.1 sccm)	Ar/159 sccm; O ₂	N/A	RF-APPJ	1 W	60~120 nm/min
Yang <i>et al.</i> , 2009	Ar (3.3 slm)	HMDSN	Ar/4.5sccm; O ₂	25	RF-APPJ	100 W	N/A
Yoshiki <i>et al.</i> , 2006	He (1000sccm) + O ₂ (10 sccm)	*TEOS (1.73 torr)	He+O ₂	100	RF-plate	6W	230 nm/min
Huang <i>et al.</i> , 2009	Air (30 slm)	TEOS / 5g/h	Ar/1 slm	RT	16 kHz APPJ	555 W	20 nm/min
Dowling <i>et al.</i> , 2009	He (10 slm) + O ₂ (100 sccm)	*TEOS (0.01sccm)	N/A	N/A	12-25 kHz APPJ	100 W	300~800 nm/min

*Precursor was introduced into plasma region

Table 5 Properties of HMDSO.

Chemical formula	Molecular weight	Vapor pressure	Boiling point	Melting point
C ₆ H ₁₈ OSi ₂	162.38	55 Torr at 30 °C	99-100 °C	-67 °C

Table 6 Summary of the instrumentation.

Item	Description	Model	Specification
1	RF impedance analyzer	MKS V-I probe 4100	Measuring electrical properties: voltage, current, power, phase angle
2	(1) Monochromator (2) Photomultiplier tube (3) Fiber (4) Collimating lenses	(1) SP 2500 (PI Acton) (2) R928 (Hamamatsu) (3)BEW-FPC-600-0.22-1.5-UV (4) 74-UV (Ocean Optics)	(1) Grating: 180-900 nm with 1200 g/mm (2) Fiber: diameter 600 μ m
3	Atomic force microscope (AFM)	Veeco Dimension 5000 Scanning Probe Microscope (D5000)	(1) Surface profile measurement (2) Tapping mode was used
4	Scanning electron microscopy (SEM)	Hitachi S-4700I	(1) Electron voltage: 0.5-30 kV (2) Amplification factor: 500k
5	Fourier transform infrared (FTIR) spectroscopy	Perkin Elmer RX1	Infrared absorption (400-4000 cm^{-1})
6	X-ray photoelectron spectroscopy (XPS)	1600 ECSA (PHI)	(1)Analyzing the surface element and compound; (2)Sample was cleaned by ion gun sputtering for 30 s
7	Contact angle machine	GH100 (KRUSS)	(1) Measuring the hydrophobic properties (2) Used a 10 μ L drop of de-ionized water
8	Pencil hardness test	B-3084T	500 g (6B-6H)

Table 7 Test conditions of RF-APPJ for SiO_x deposition.

Discharge gas	Ar; Ar + (0 ~ 10 %) O ₂
Flow rate	5 slm (18.3 m/s)
Dielectric material	Quartz 4×6 mm (t=1 mm)
Carrier gas flow rate for HMDSO	Ar-0.1 slm (0.83 m/s) HMDSO (4g/h)
Treatment distance	3 ~ 7.5 mm
Input power	35 ~ 50 W
Treatment sample	Si P-type (100) 6 inch
Substrate temperature	Room temperature ~ 300 °C
Moving stage	10 mm/sec
Treatment passes	2~200 passes

Table 8 Pencil hardness results of SiO_x films.

Parameter	Deposition rate of T _{sub} = 200 °C	Thickness (nm)	Pencil hardness	Deposition rate of T _{sub} = 300 °C	Thickness (nm)	Pencil hardness
Ar	90 nm/min	100	5H	37.5 nm/min	100	5H
		300	5H			
Ar+0.2%O ₂	600 nm/min	100	2H	200 nm/min	100	5H
		300	H			
Ar+0.8%O ₂	1200 nm/min	100	HB	275 nm/min	100	4H
		300	HB			

Table 9 Elemental composition of SiO_x under various oxygen concentrations.

Parameter	C (%)	O (%)	Si (%)	O/Si ratio	C/O ratio
Ar	18.3	46.4	35.5	1.3	0.4
Ar + 0.2 % O ₂	16.6	46.4	36.1	1.31	0.35
Ar + 0.8 % O ₂	15.5	48.9	35.6	1.38	0.32
Ar + 4 % O ₂	15.6	51.4	33.0	1.56	0.3
Ar + 10 % O ₂	13.9	51.9	34.2	1.52	0.27

* 200 °C Substrate temperature

Table 10 Elemental composition of SiO_x under various substrate temperatures.

Substrate temperature (°C)	C (%)	O (%)	Si (%)	O/Si ratio	C/O ratio
25	23.84	42.41	33.75	1.26	0.56
100	17.16	48.43	34.41	1.41	0.35
200	12.8	52.92	34.26	1.55	0.24
300	10.51	54.1	35.39	1.53	0.19

* Oxygen concentration: 4 %

Figure

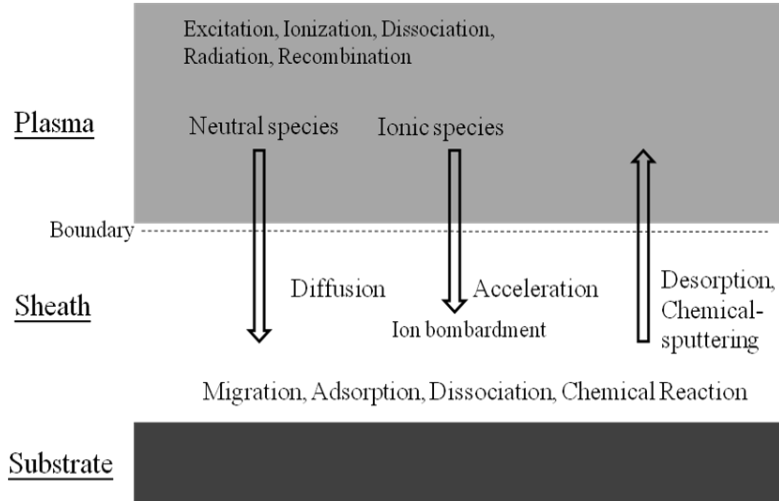


Figure 1.1 Schematic representation of the PECVD reaction process [Konuma, 2005].

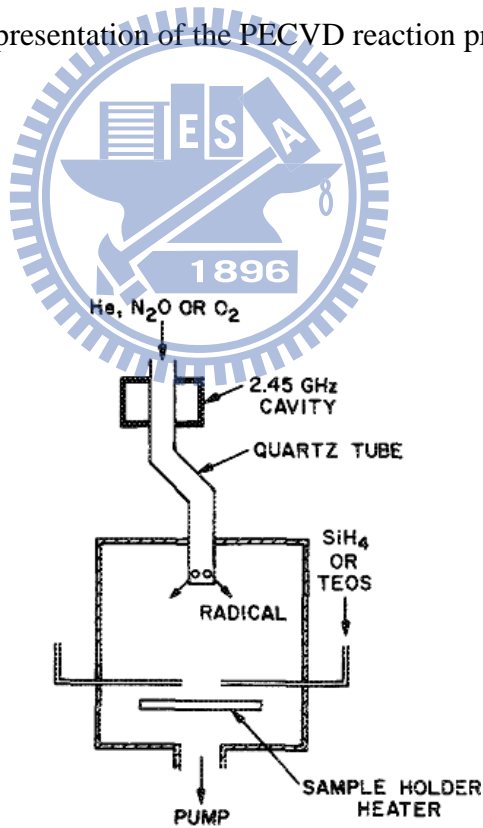


Figure 1.2 The system configuration for LP-PECVD reactor [Pai *et al.*, 1990].

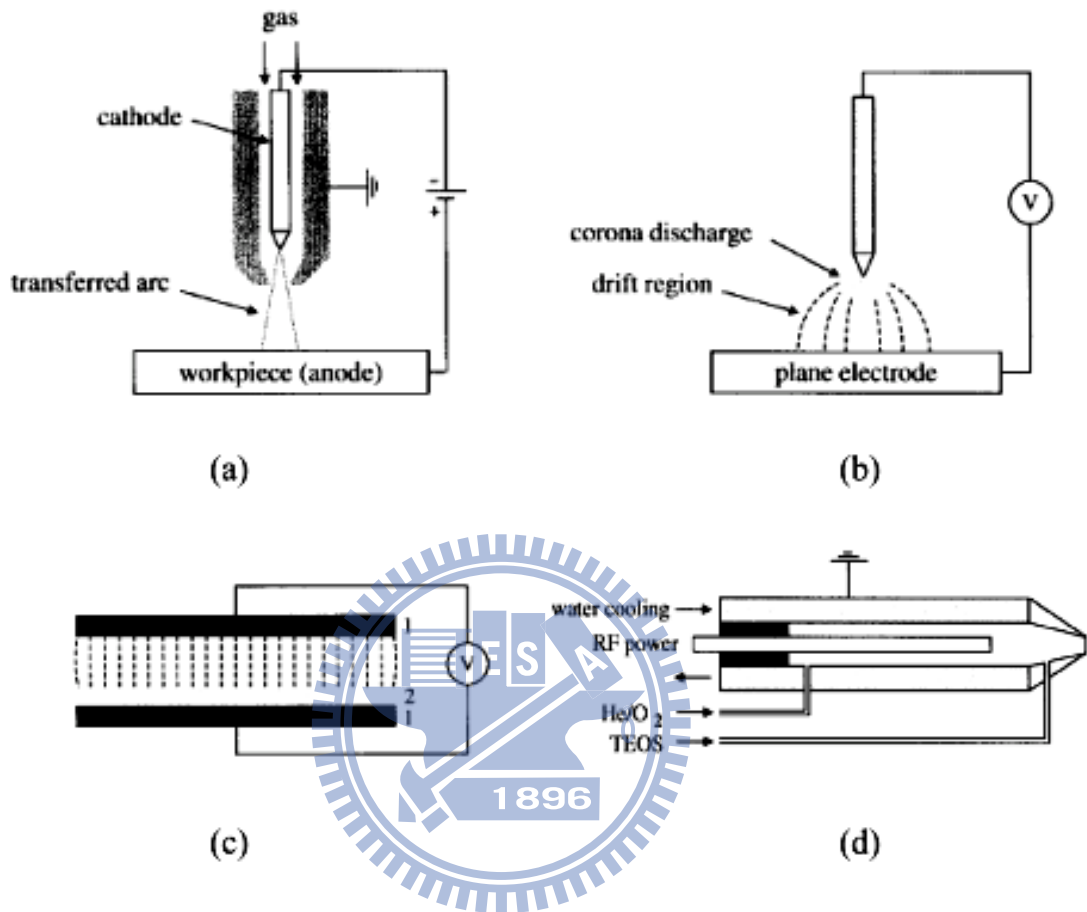


Figure 1.3 Types of atmospheric pressure plasma. (a) Transferred arc; (b) Corona discharge; (c) Dielectric barrier discharge; (d) Plasma jet [Schutz *et al.*, 1998].

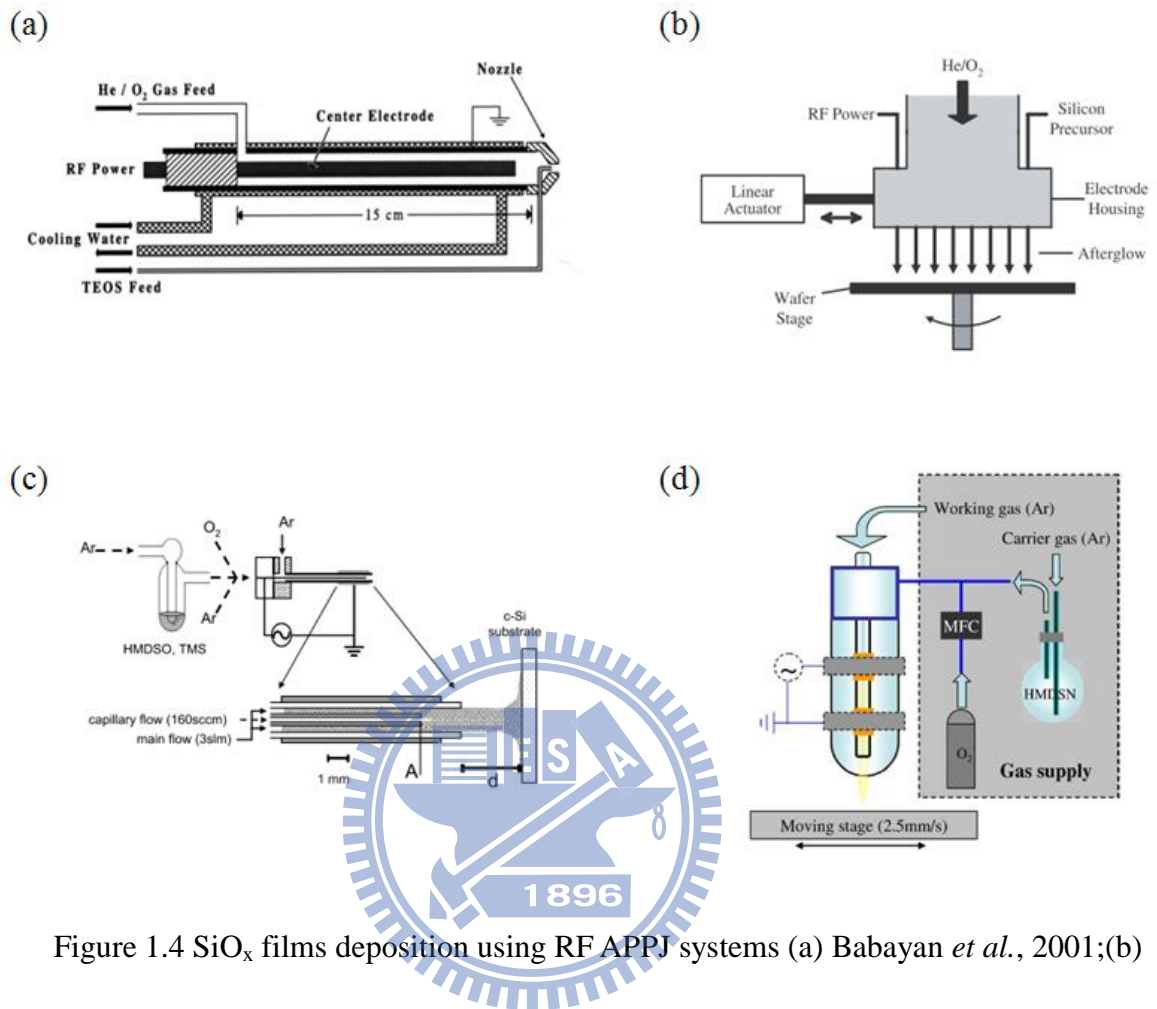


Figure 1.4 SiO_x films deposition using RF APPJ systems (a) Babayan *et al.*, 2001;(b)

Nowling *et al.*,2005; (c) Raballand *et al.*, 2009; (d) Yang *et al.*, 2009.

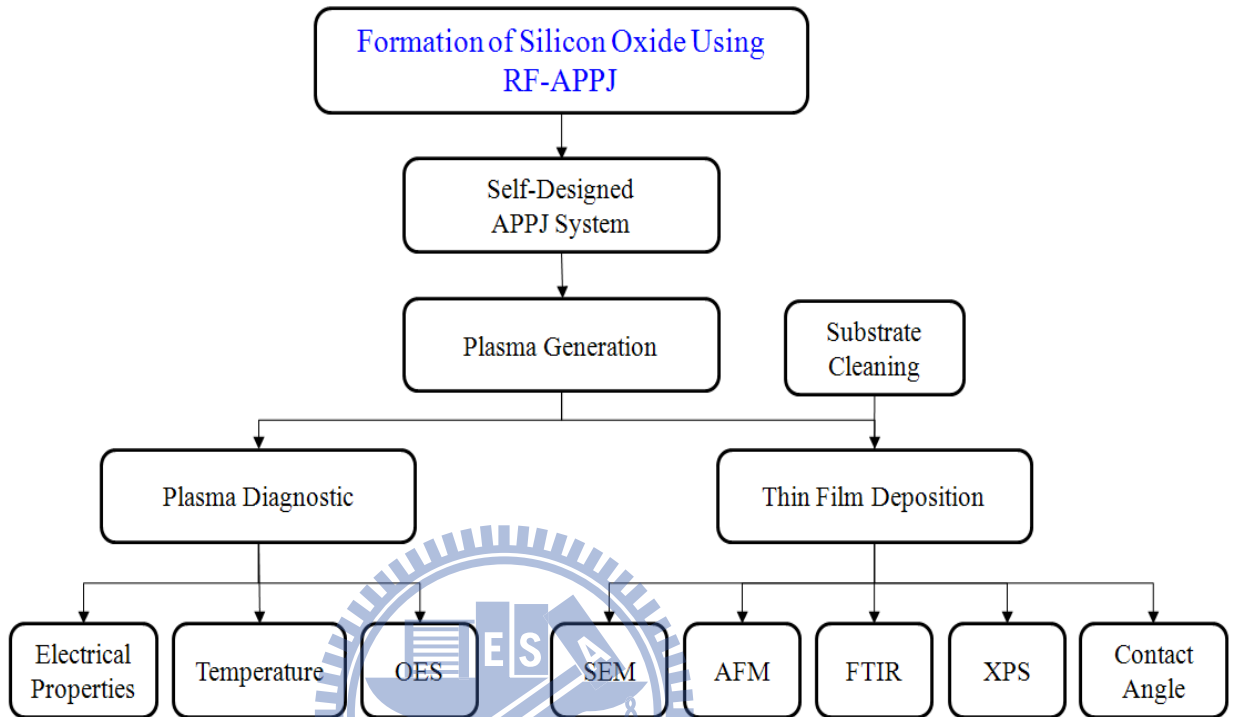


Figure 2.1 Process flow chart.

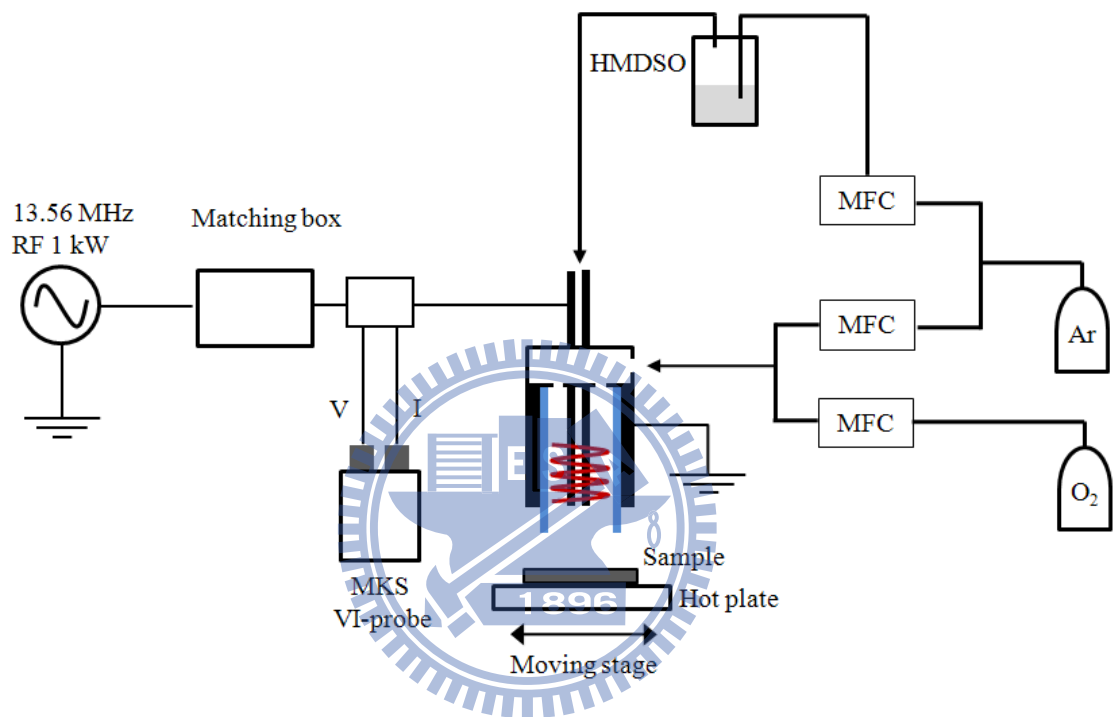


Figure 2.2 Overview of the atmospheric pressure plasma jet system.

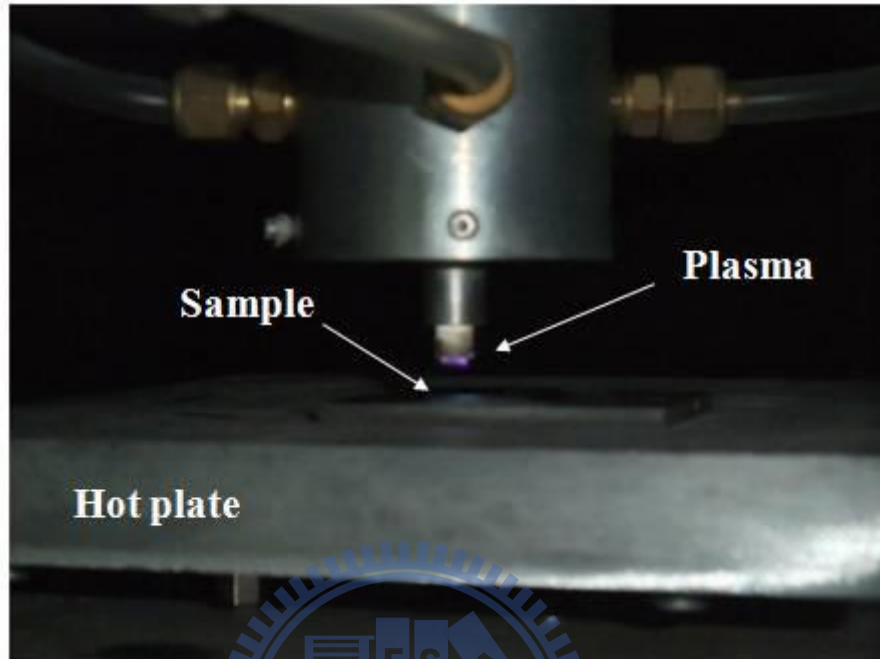


Figure 2.3 Processing of thin film deposition.

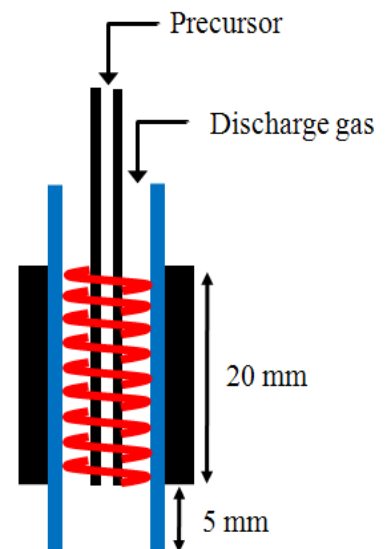


Figure 2.4 The schematic diagram of electrode configuration.



Figure 2.5 RF power supply.

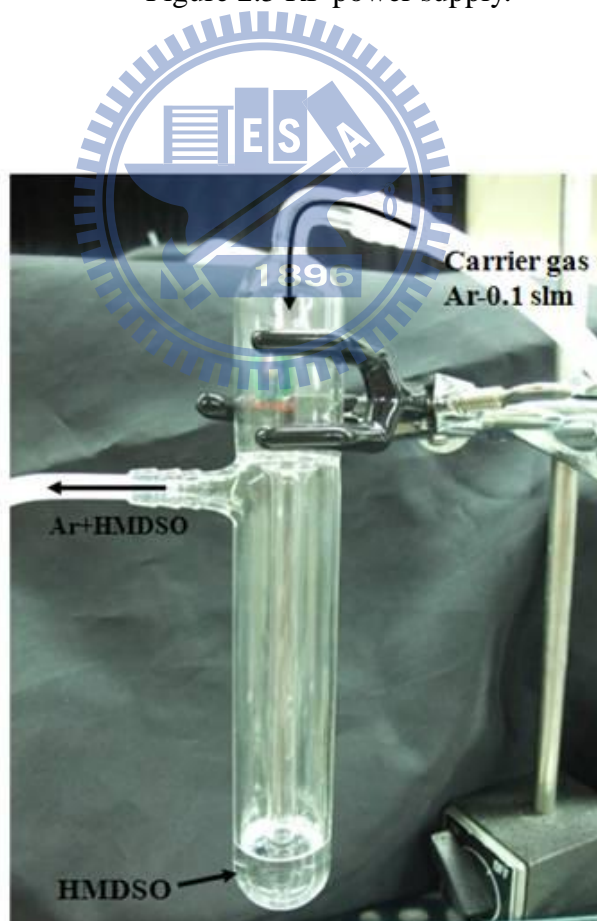


Figure 2.6 Bubbler for liquid precursor.

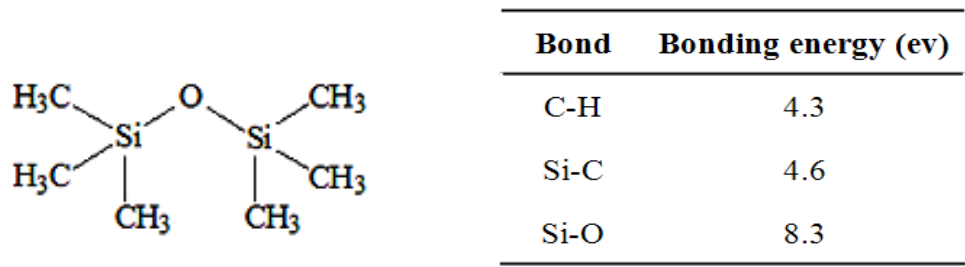


Figure 2.7 HMDSO monomer structure and bond strengths.



Figure 2.8 Optical emission spectroscopy.



Figure 2.9 Scanning electron microscopy.



Figure 2.10 Atomic force microscopy.

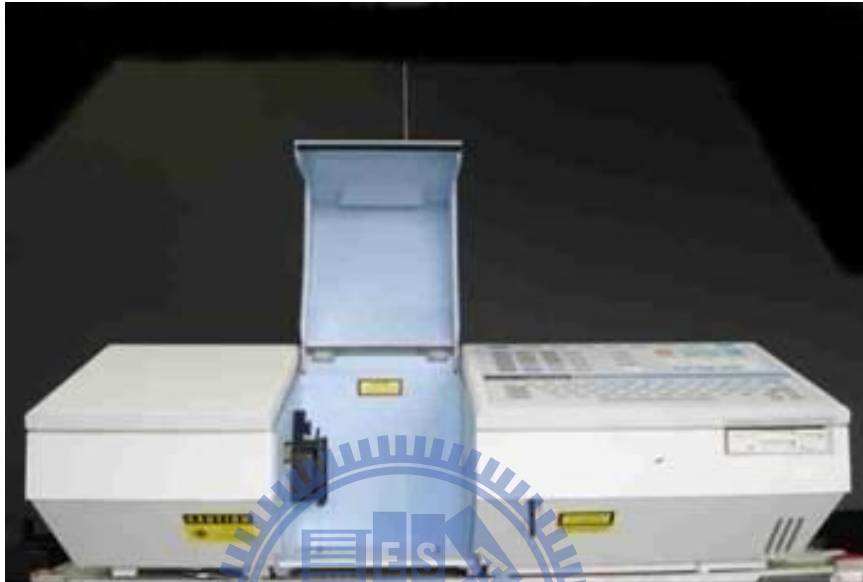


Figure 2.11 Fourier transform infrared (FTIR) spectroscopy

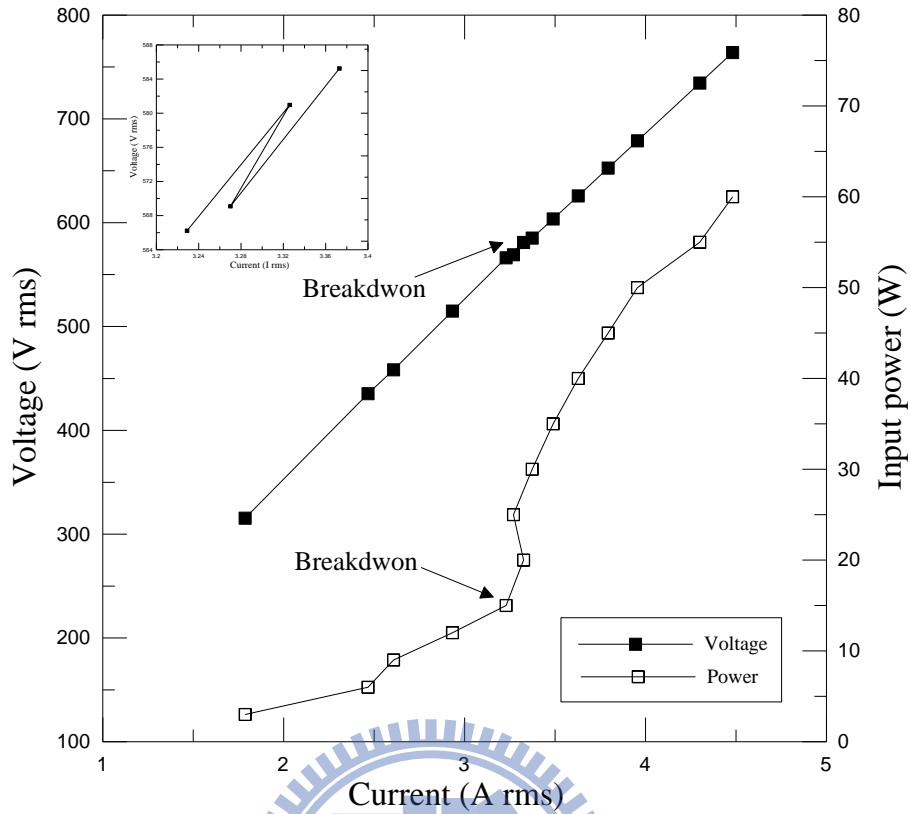


Figure 3.1 I-V-P curve of pure argon discharge (Ar flow rate: 5 slm).

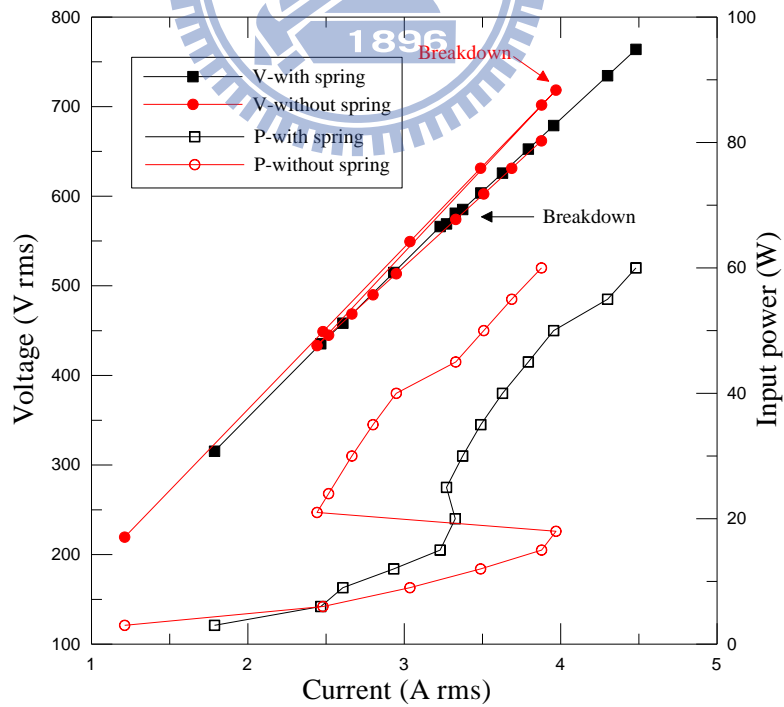


Figure 3.2 I-V curves of Ar discharge with and without spring (Ar flow rate: 5 slm).

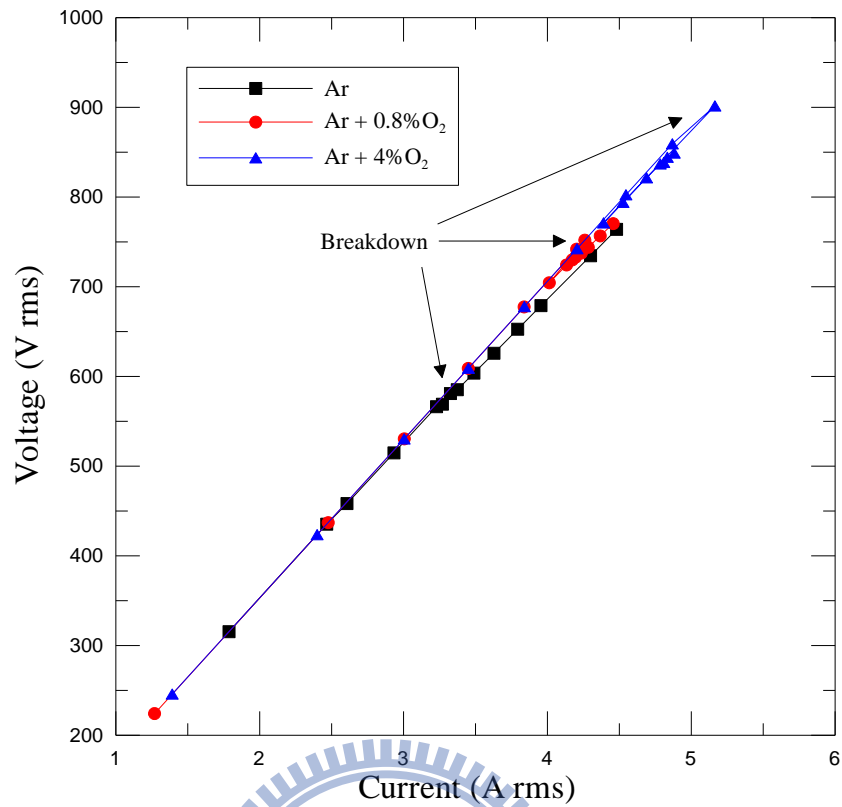


Figure 3.3 I-V curves of Ar, Ar+0.8%O₂, and Ar+4% O₂ discharge (Ar flow rate: 5 slm).

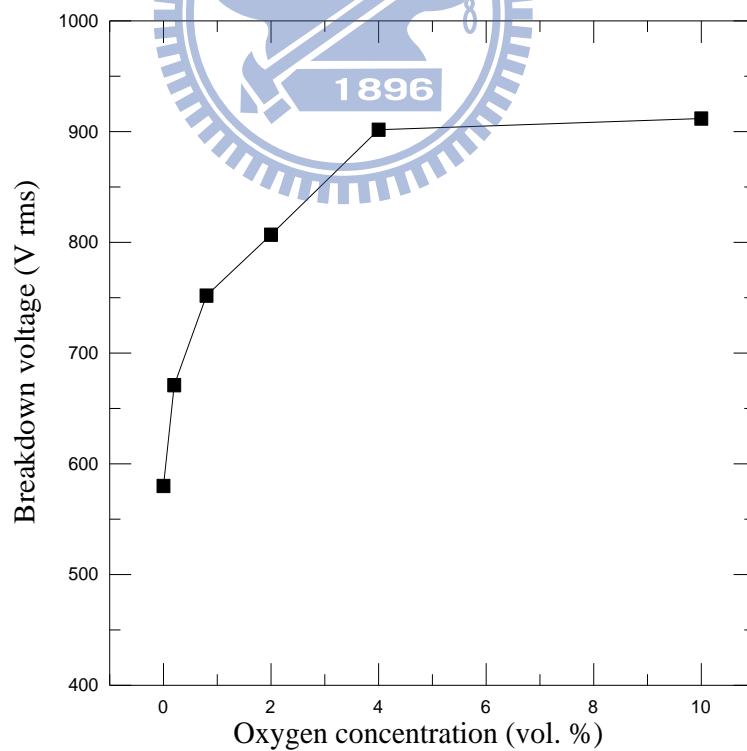


Figure 3.4 Breakdown voltage of the argon plasma mixed with various oxygen concentrations (Ar flow rate: 5 slm).

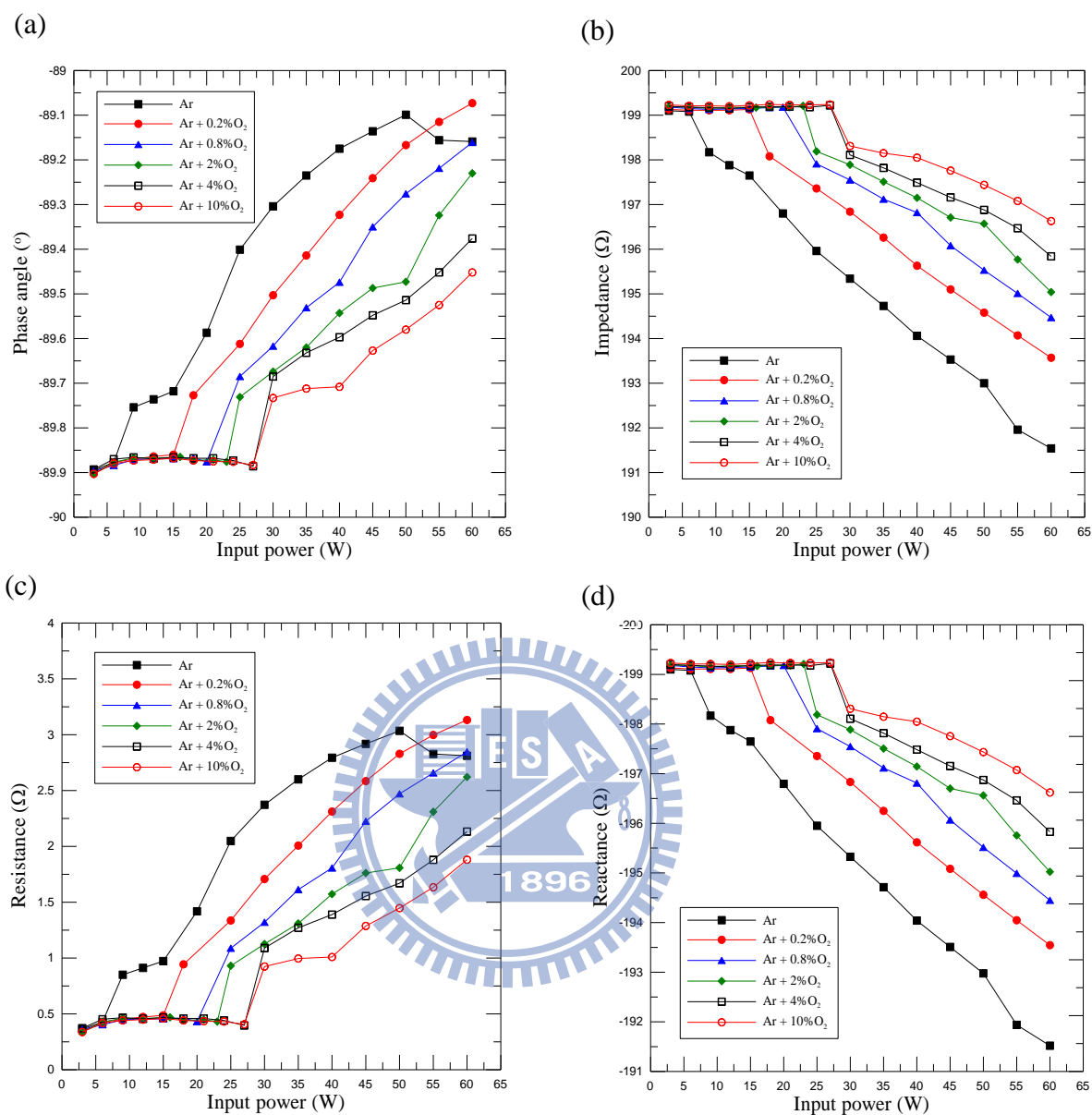


Figure 3.5 The electrical characteristics curves as a function of input power for different

oxygen added into argon plasma (a) P- θ ; (b) P-Impedance; (c) P-Resistance; (d)

P-Reactance (Ar flow rate: 5 slm).

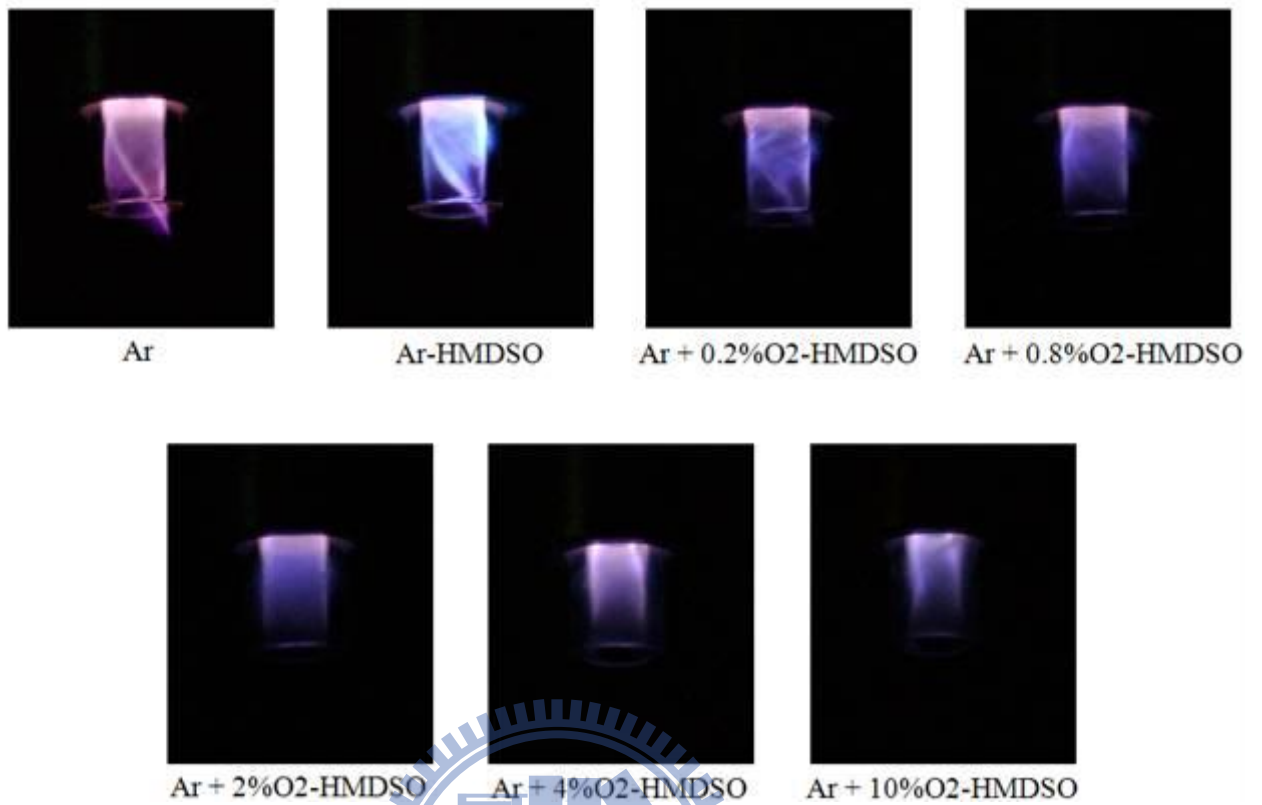


Figure 3.6 Images for argon mixed with different concentrations of oxygen plasma and HMDSO introduced into downstream of discharge region (Ar flow rate: 5 slm; RF power: 50 W).

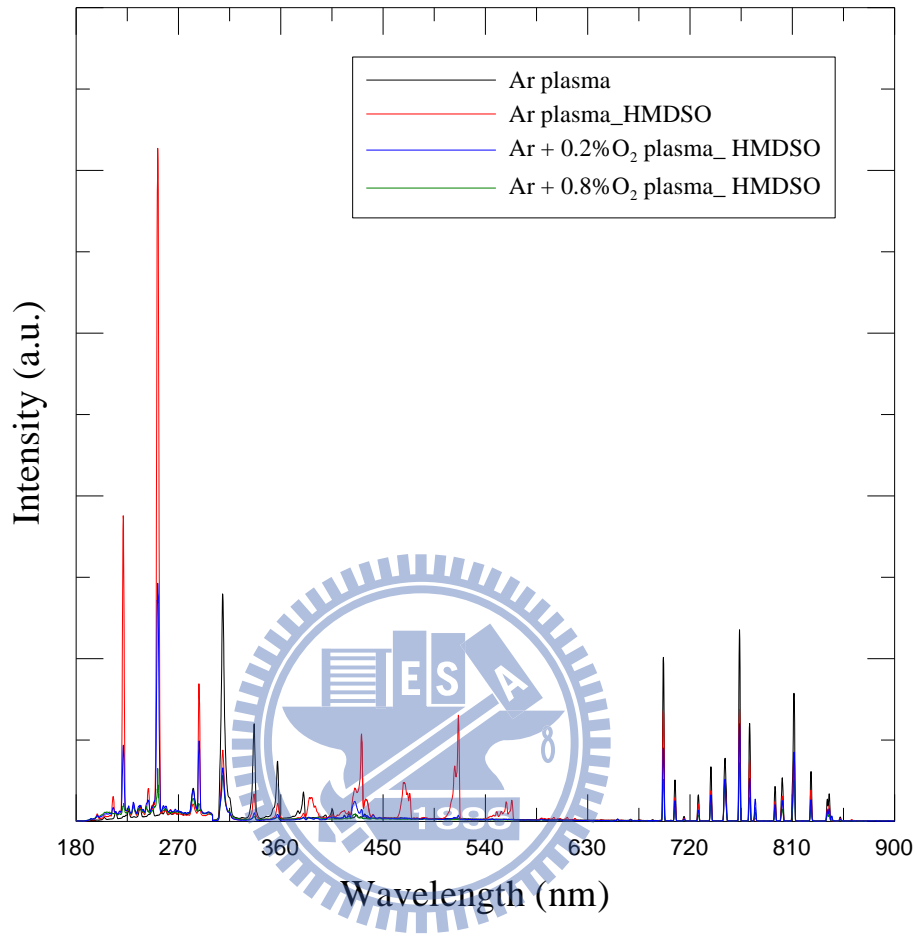


Figure 3.7 OES of argon mixed with different concentrations of oxygen plasma and HMDSO introduced into downstream of discharge region (Ar flow rate: 5 slm; RF power: 50 W).

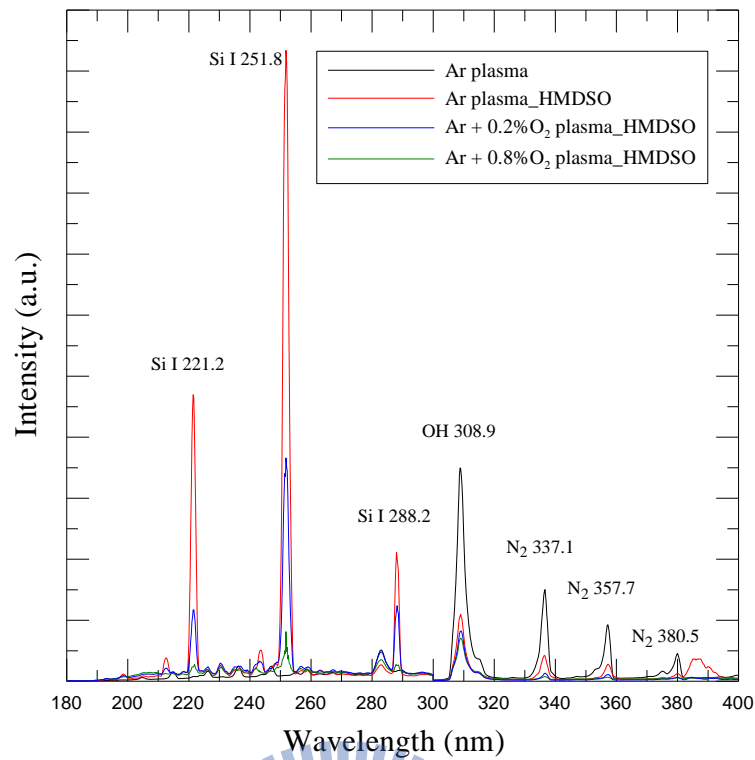


Figure 3.8 OES of argon mixed with different concentrations of oxygen plasma and HMDSO introduced into downstream of discharge region at 180 to 400 nm (Ar flow rate: 5 slm; RF power: 50 W).

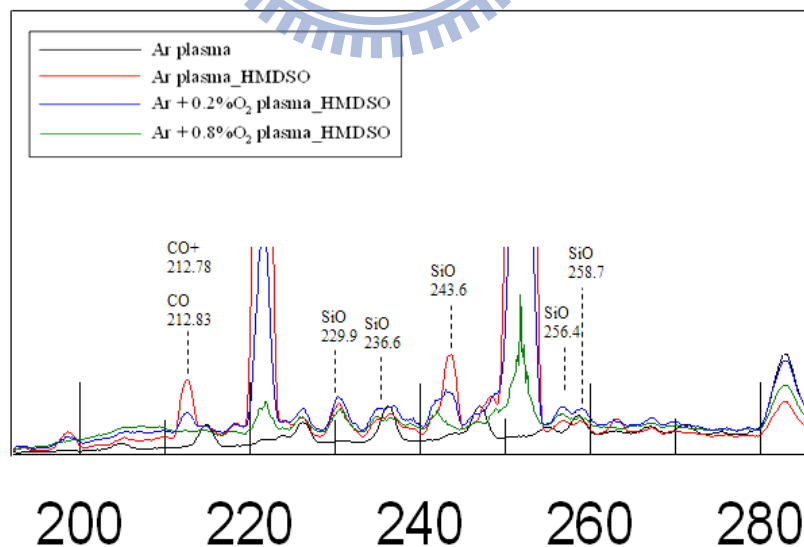


Figure 3.9 Species emitted of HMDSO dissociation (Ar flow rate: 5 slm; RF power: 50 W).

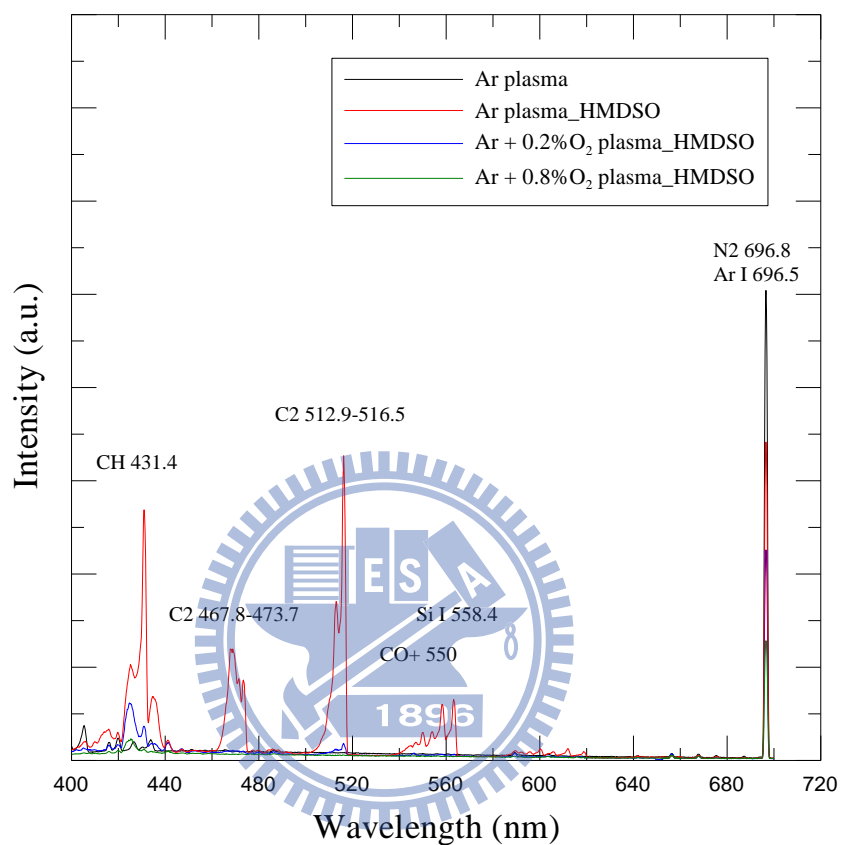


Figure 3.10 OES of argon mixed with different concentrations of oxygen plasma and HMDSO introduced into downstream of discharge region at 400 to 700 nm (Ar flow rate: 5 slm; RF power: 50 W).

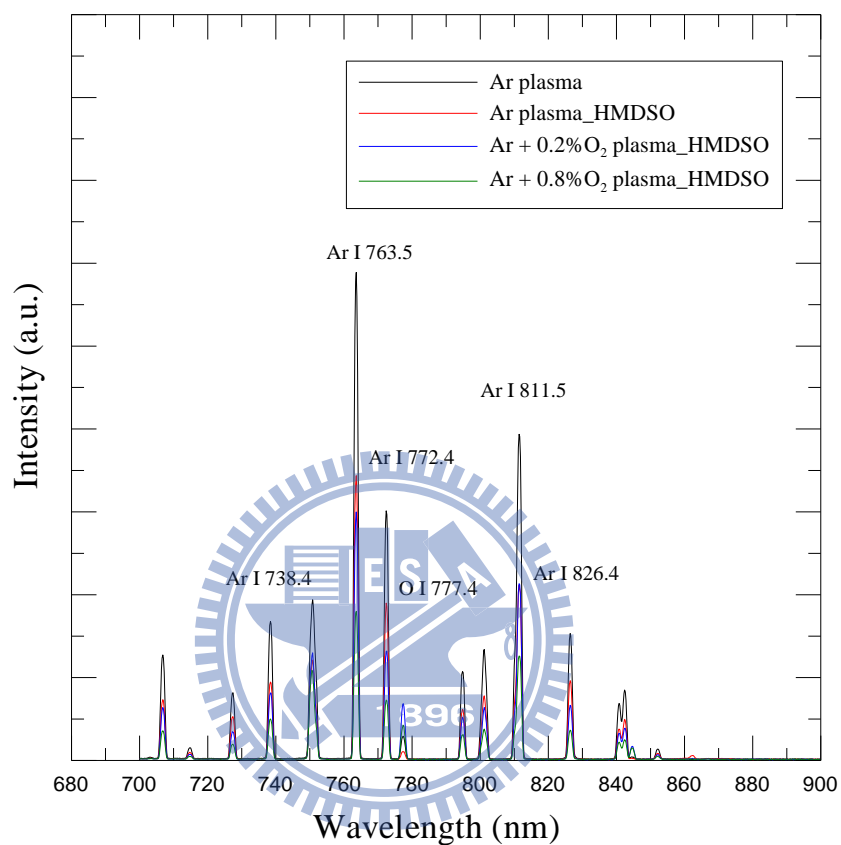


Figure 3.11 OES of argon mixed with different concentrations of oxygen plasma and HMDSO introduced into downstream of discharge region at 700 to 900 nm (Ar flow rate: 5 slm; RF power: 50 W).

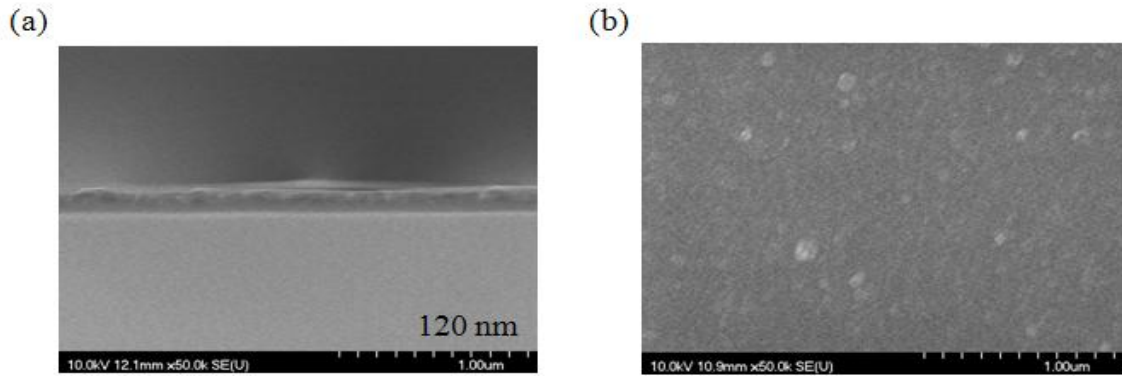


Figure 3.12 SEM images of SiO_x thin film (a) cross section; (b) surface morphology on the 50 W RF power, 200 °C substrate temperature, 0 % oxygen concentration, 5 mm treatment distance and 200 passes.

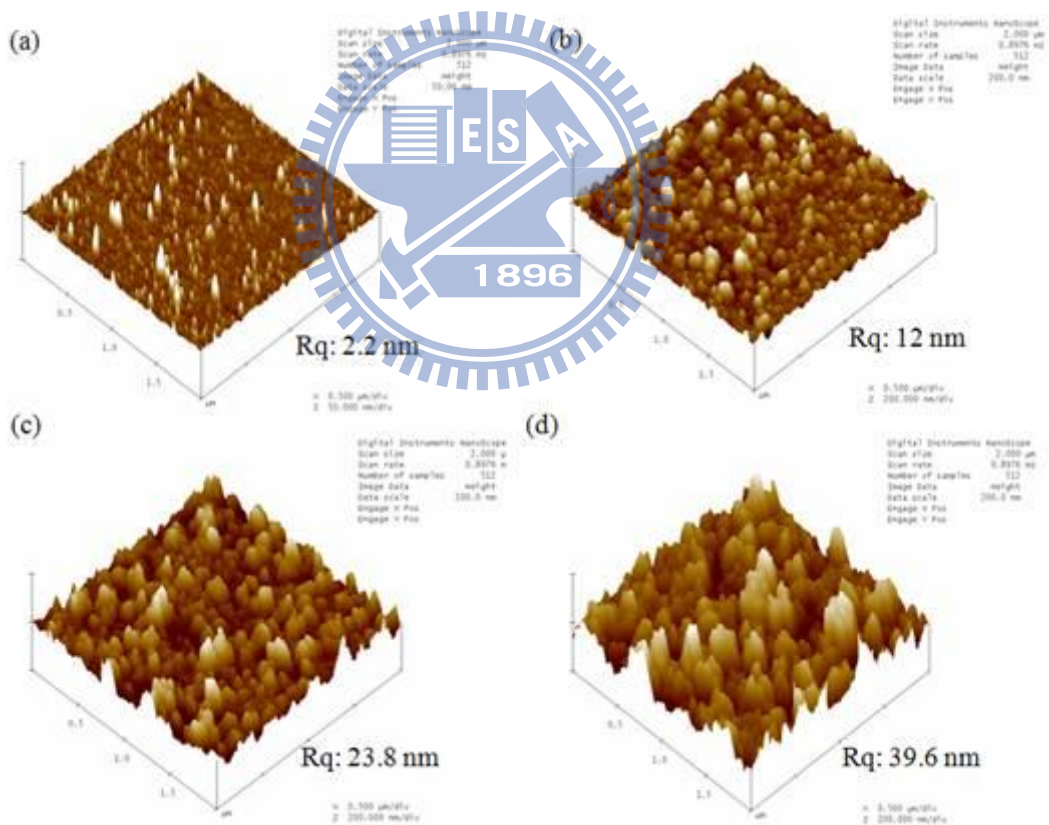


Figure 3.13 AFM of SiO_x were deposited at different treatment passes (a) 4 passes; (b) 10 passes; (c) 20 passes; (d) 30 passes on the 50 W RF power, 200 °C substrate temperature, 0.8 % oxygen concentration, and 5 mm treatment distance.

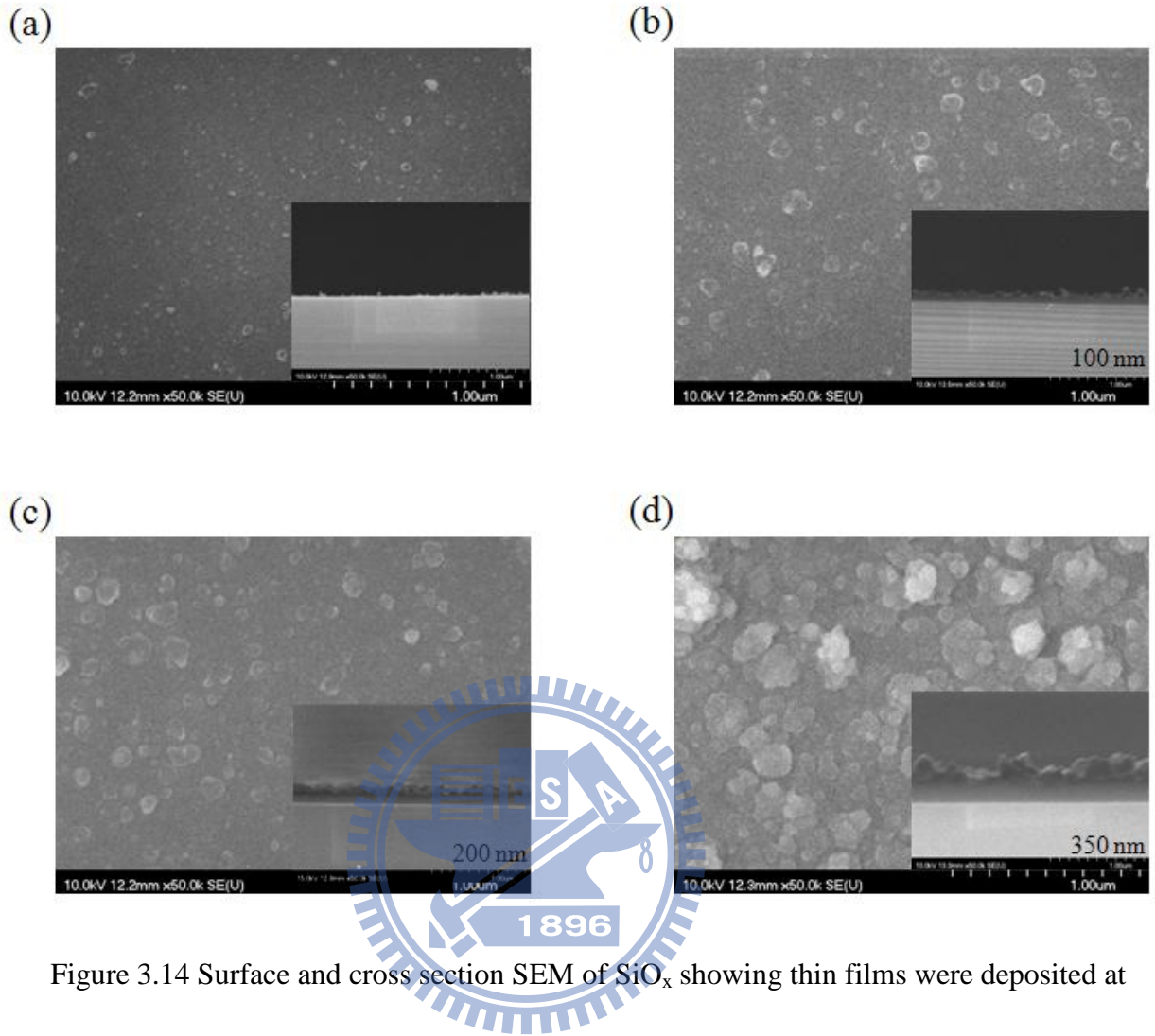


Figure 3.14 Surface and cross section SEM of SiO_x showing thin films were deposited at different treatment passes (a) 4 passes; (b) 10 passes; (c) 20 passes; (d) 30 passes on the 50 W RF power, 200 °C substrate temperature, 0.8 % oxygen concentration, and 5 mm treatment distance.

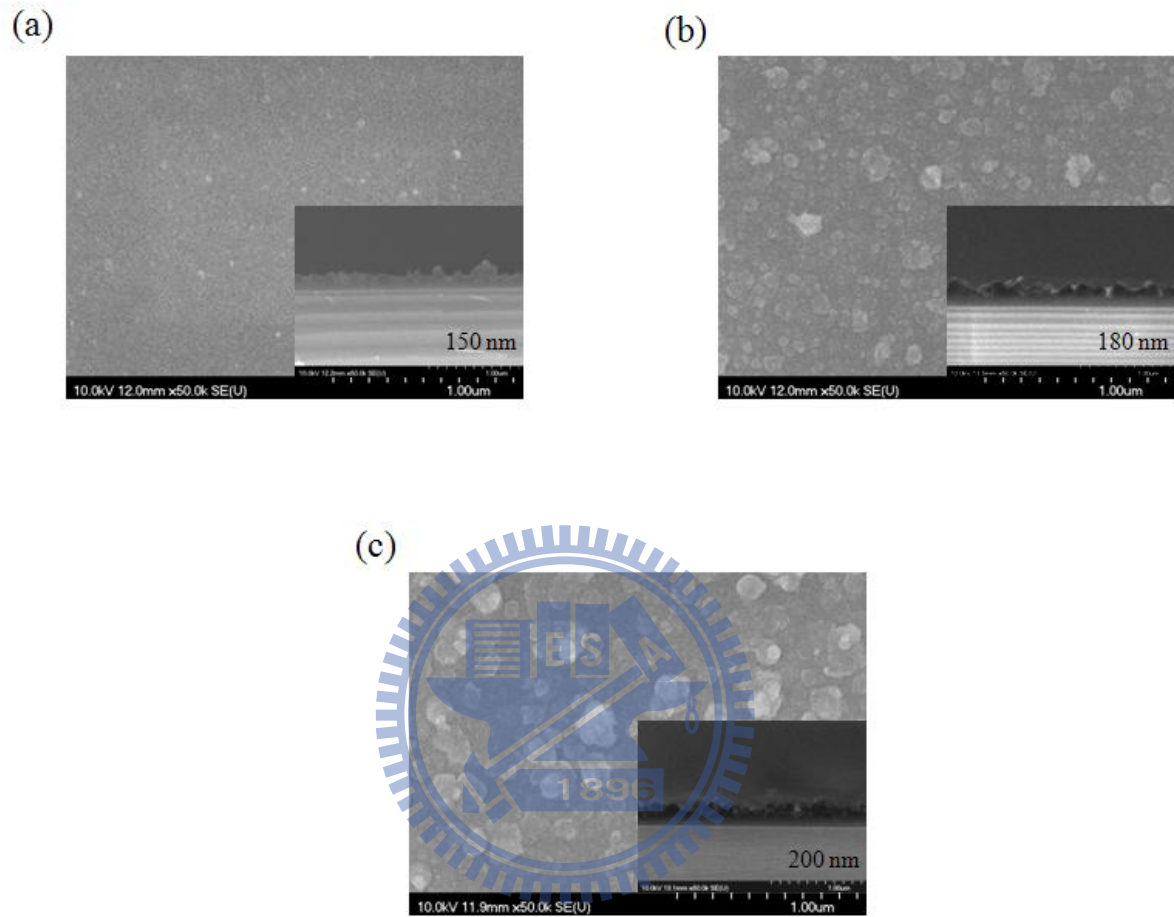


Figure 3.15 Surface and cross section SEM of SiO_x showing thin films were deposited in different RF power (a) 35 W; (b) 40 W; (c) 50 W on 200 °C substrate temperature, 0.8 % oxygen concentration, 5 mm treatment distance and 20 passes.

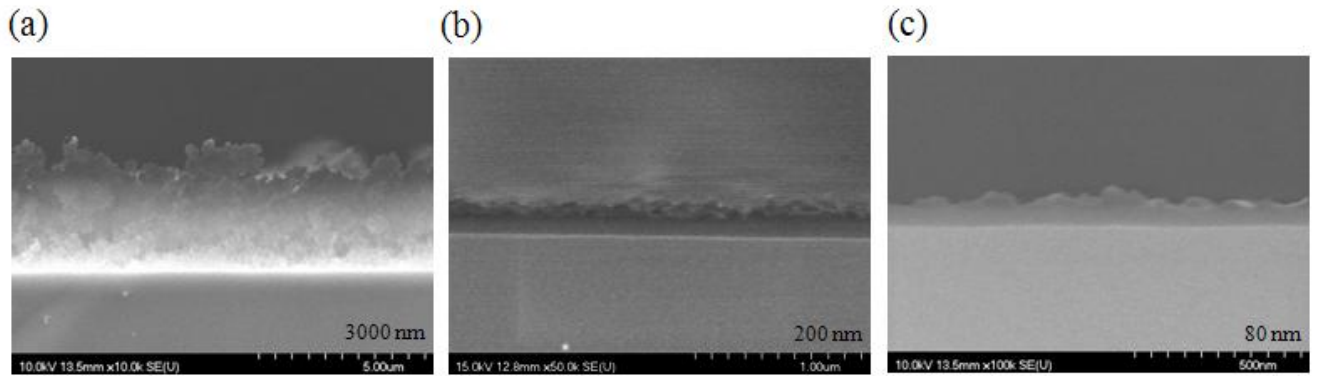


Figure 3.16 Cross section SEM of SiO_x showing thin films were deposited at different treatment distance (a) 3 mm; (b) 5 mm; (c) 7.5 mm on 50 W RF power, 200 °C substrate temperature, 0.8 % oxygen concentration, and 20 passes.

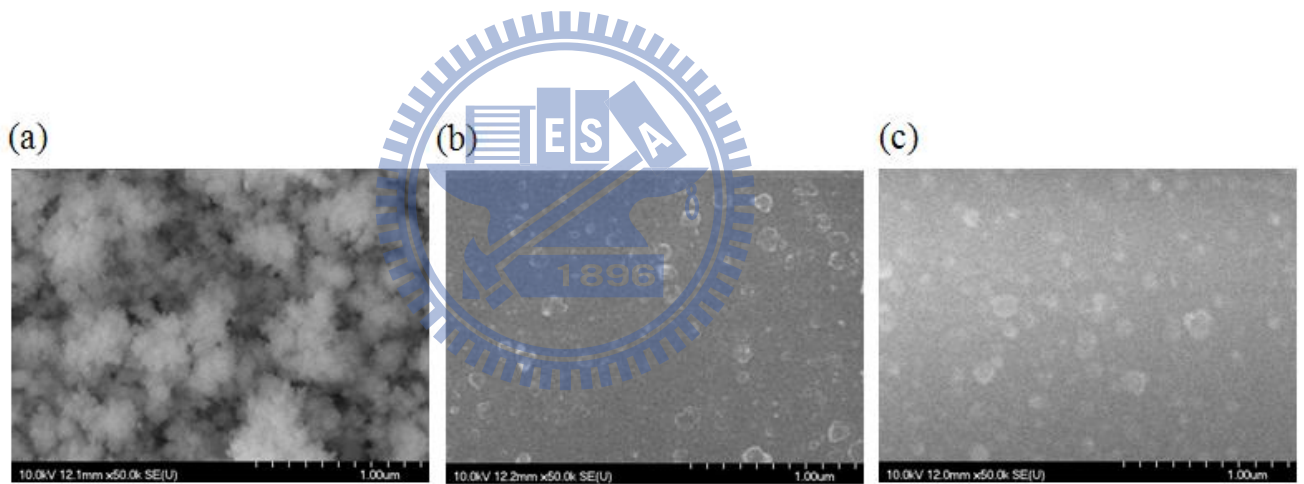


Figure 3.17 Surface SEM of SiO_x showing thin films were deposited at different treatment distance (a) 3 mm; (b) 5 mm; (c) 7.5 mm on 50 W RF power, 200 °C substrate temperature, 0.8 % oxygen concentration, and 20 passes.

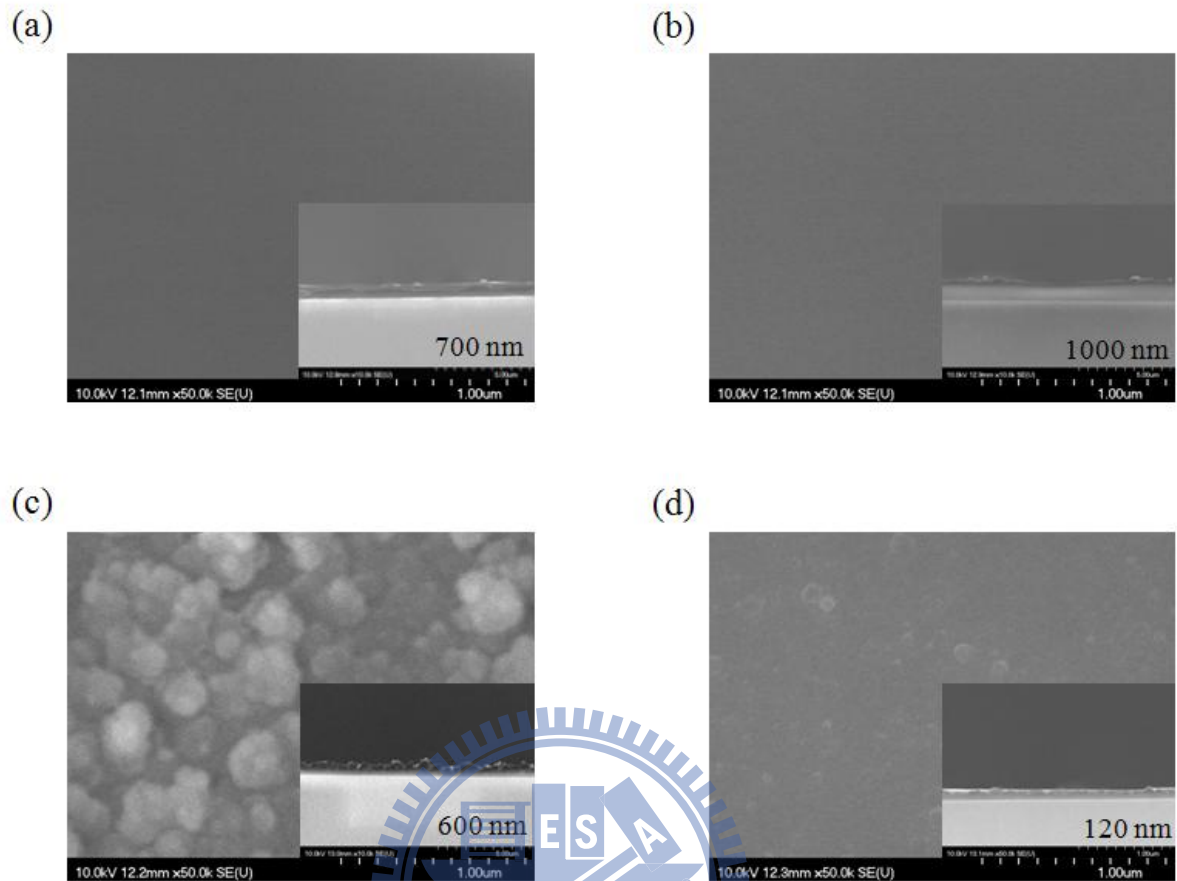


Figure 3.18 Surface and cross section SEM of SiO_x showing thin films were deposited on the different substrate temperatures (a) 25 °C; (b) 100 °C; (c) 200 °C (d) 300 °C on 50 W RF power, 0.8 % oxygen concentration, 5 mm treatment distance and 60 passes.

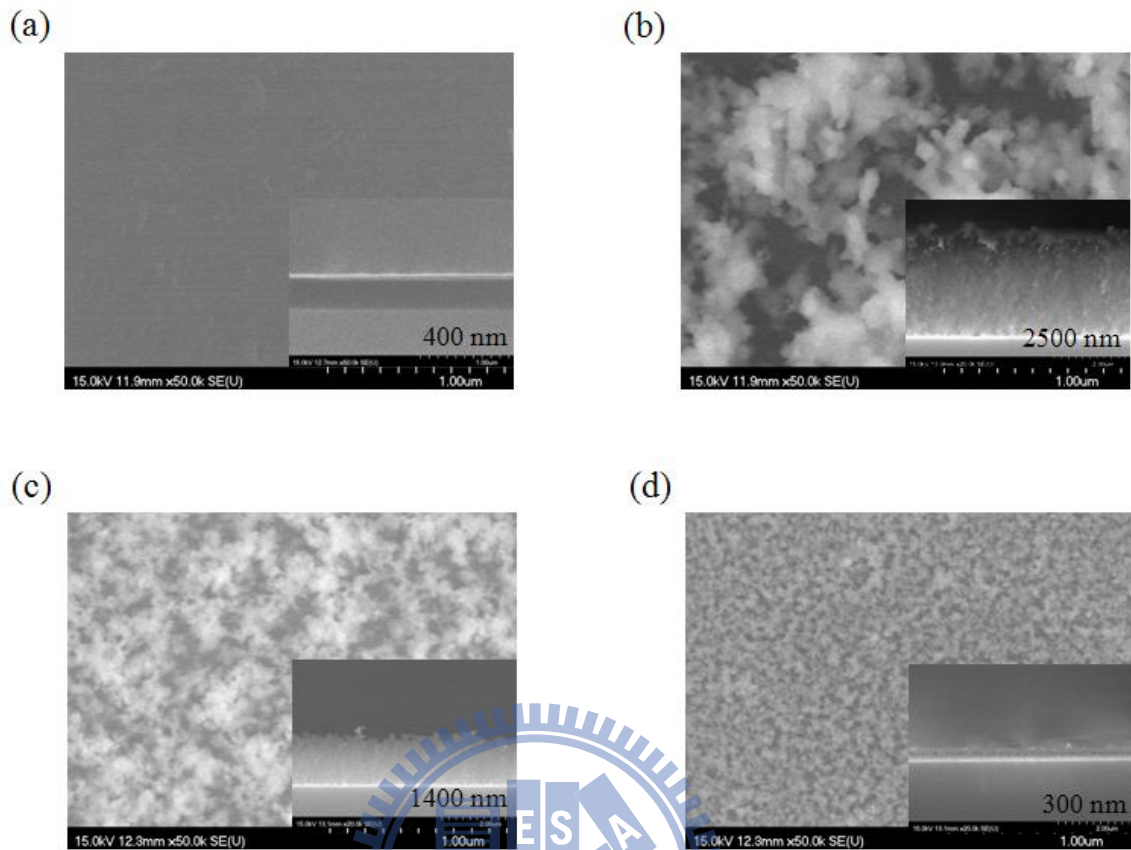
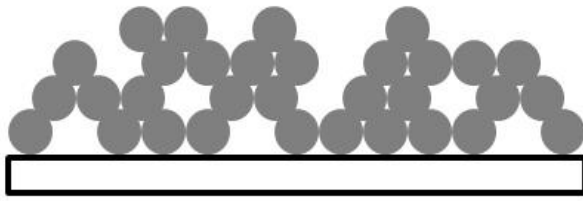
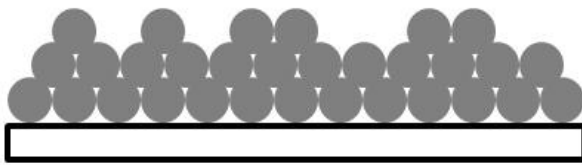
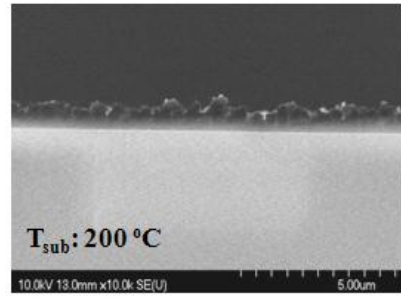


Figure 3.19 Surface and cross section SEM of SiO_x showing thin films were deposited on the different substrate temperatures (a) 25 °C; (b) 100 °C; (c) 200 °C (d) 300 °C on 50 W RF power, 4 % oxygen concentration, 5 mm treatment distance and 20 passes.



Low substrate temperature



High substrate temperature

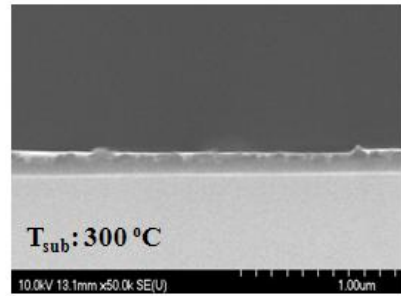


Figure 3.20 The schematic diagram of influence of substrate temperature.



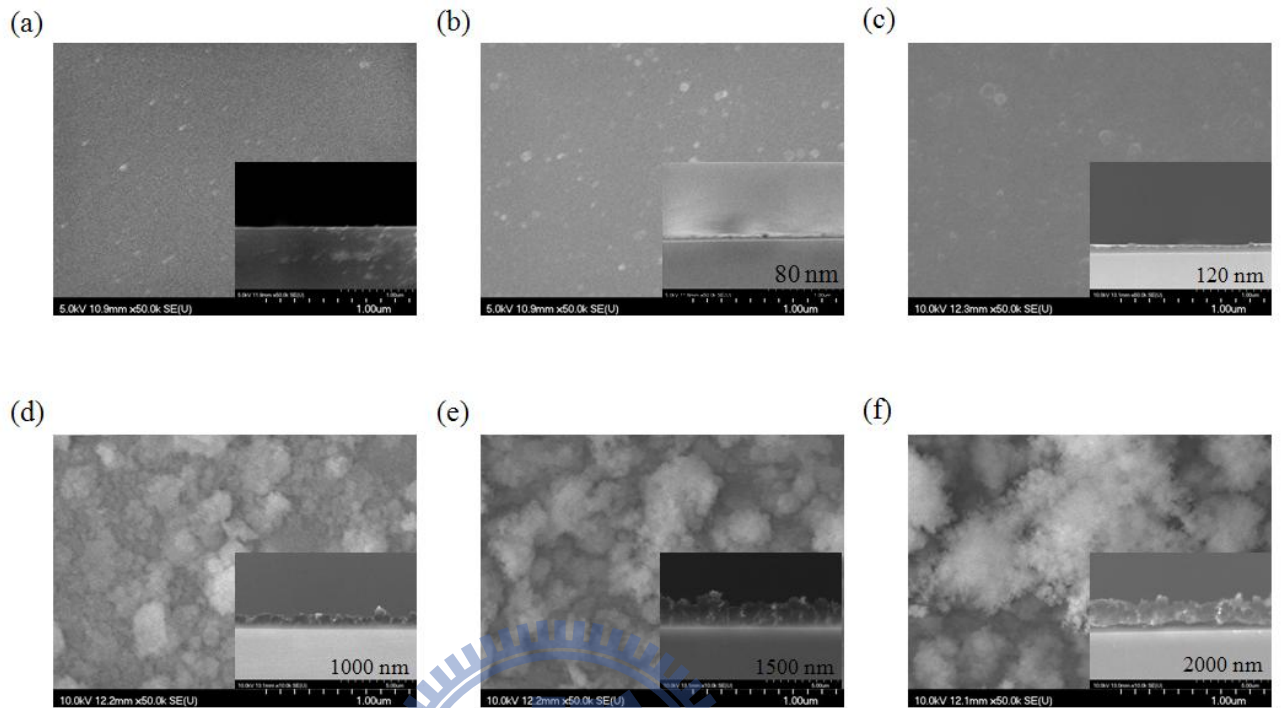


Figure 3.21 Surface and cross section SEM of SiO_x showing thin films were deposited using argon plasma mixed with different oxygen concentrations (a) 0 %; (b) 0.2 %; (c) 0.8% (d) 2 %; (e) 4 %; (f) 10 % on 50 W RF power, 300 °C substrate temperature 5 mm treatment distance and 60 passes.

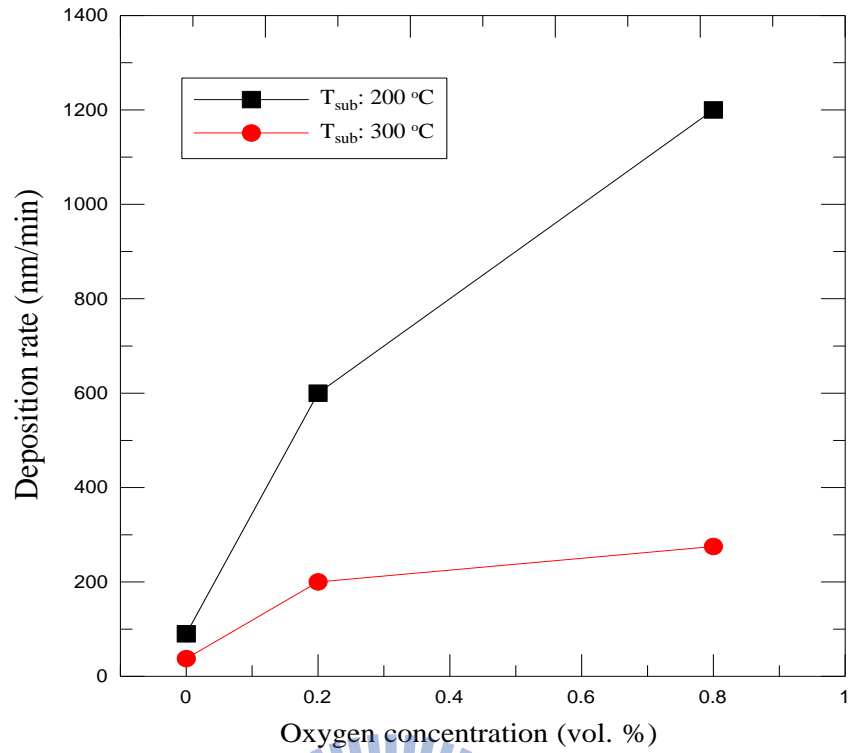
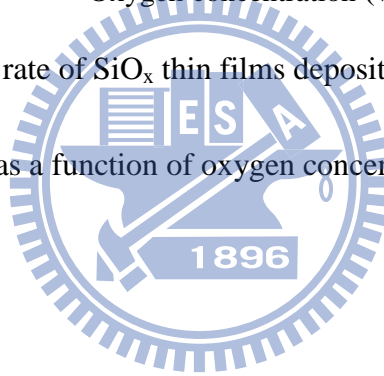


Figure 3.22 Deposition rate of SiO_x thin films deposited on the 200 and 300 °C substrate temperature as a function of oxygen concentration in the discharge.



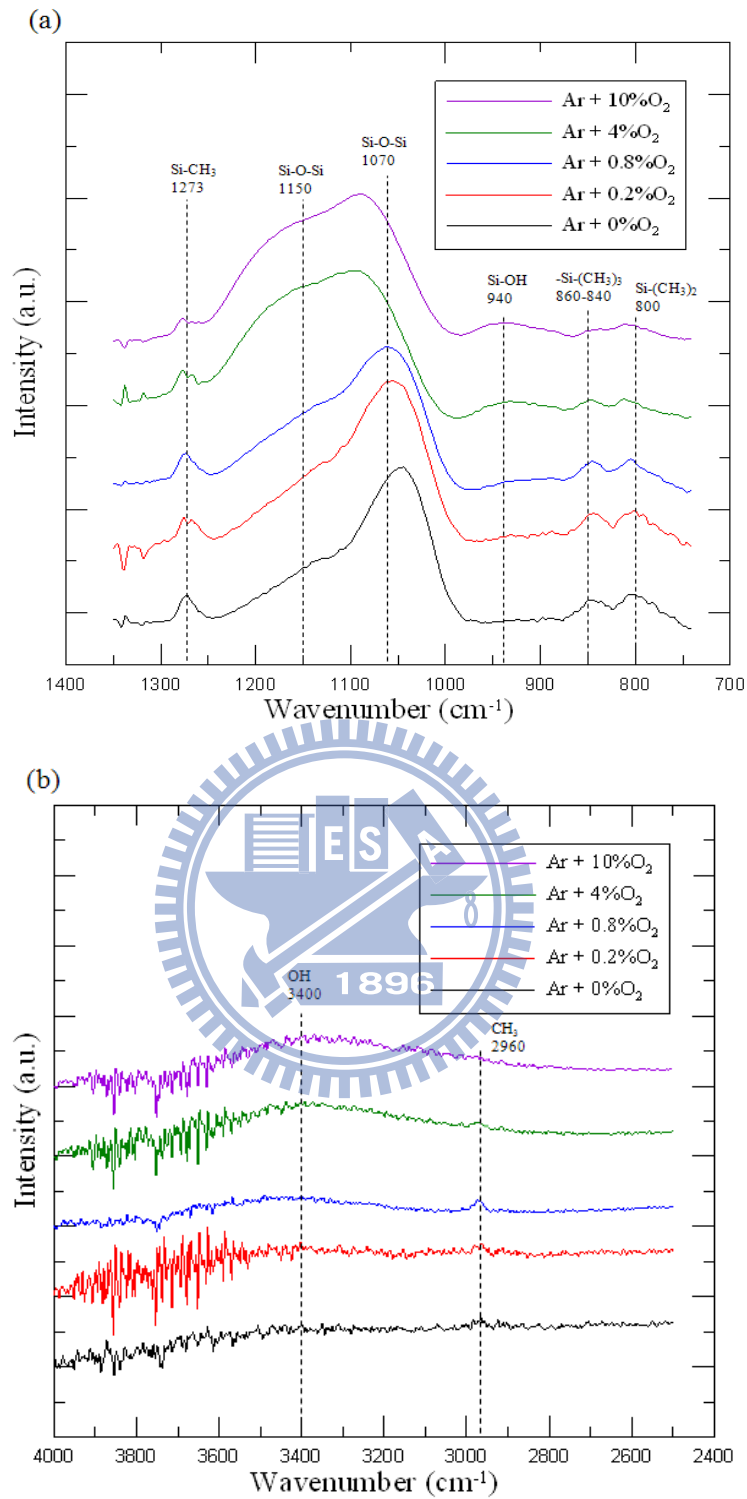


Figure 3.23 IR spectra of SiO_x thin films grown at substrate temperature 200 °C using argon plasma mixed with different oxygen concentrations (a) 1400-700 cm⁻¹; (b) 4000-2400 cm⁻¹.

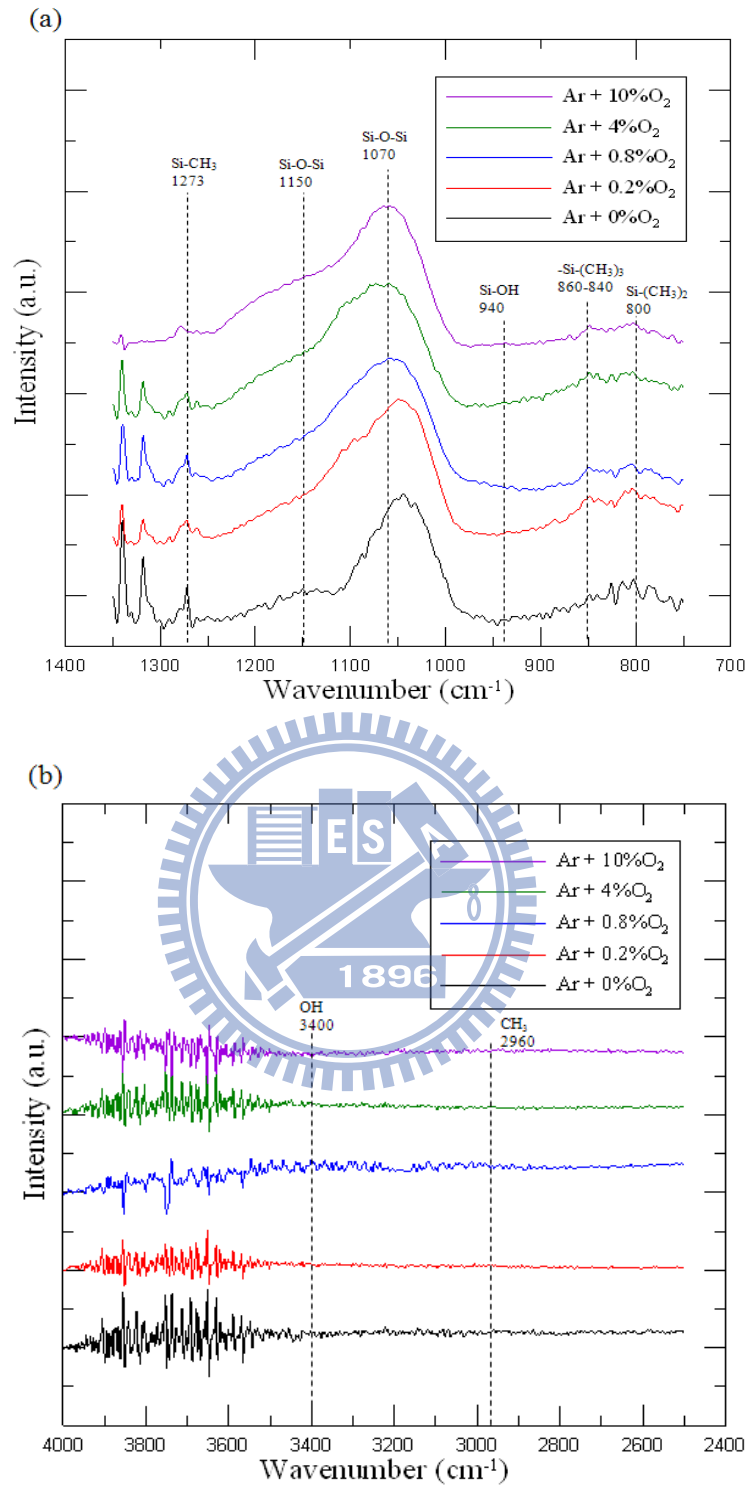


Figure 3.24 IR spectra of SiO_x thin films grown at substrate temperature 300 °C using argon plasma mixed with different oxygen concentrations (a) 1400-700 cm⁻¹; (b) 4000-2400 cm⁻¹.

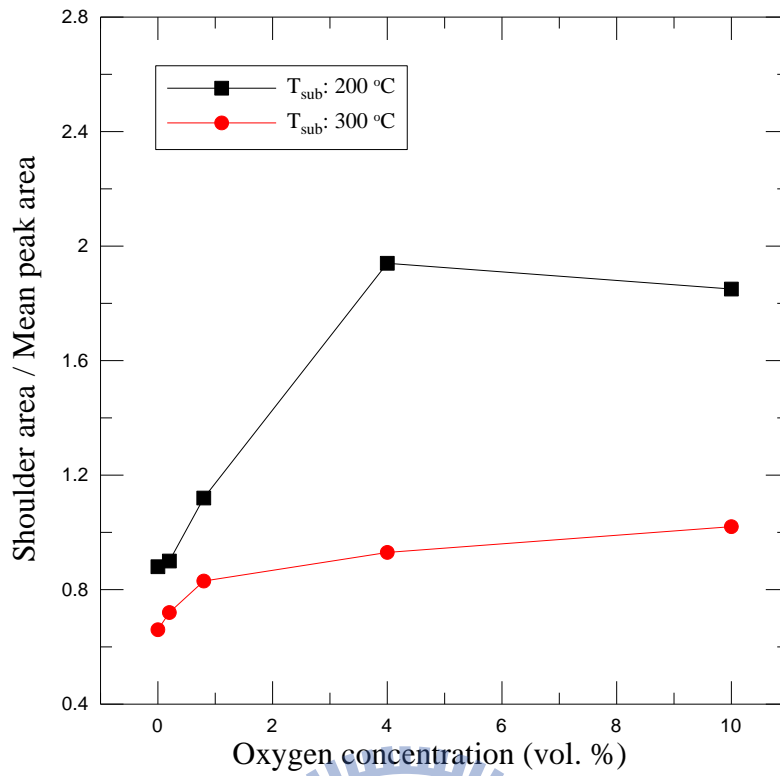
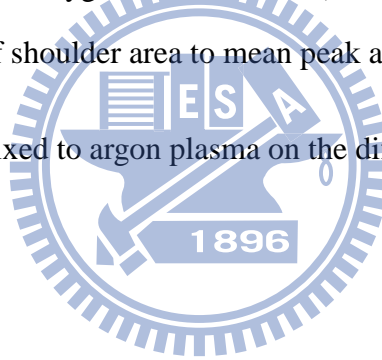


Figure 3.25 The ratio of shoulder area to mean peak area as a function of various oxygen concentrations mixed to argon plasma on the different substrate temperature.



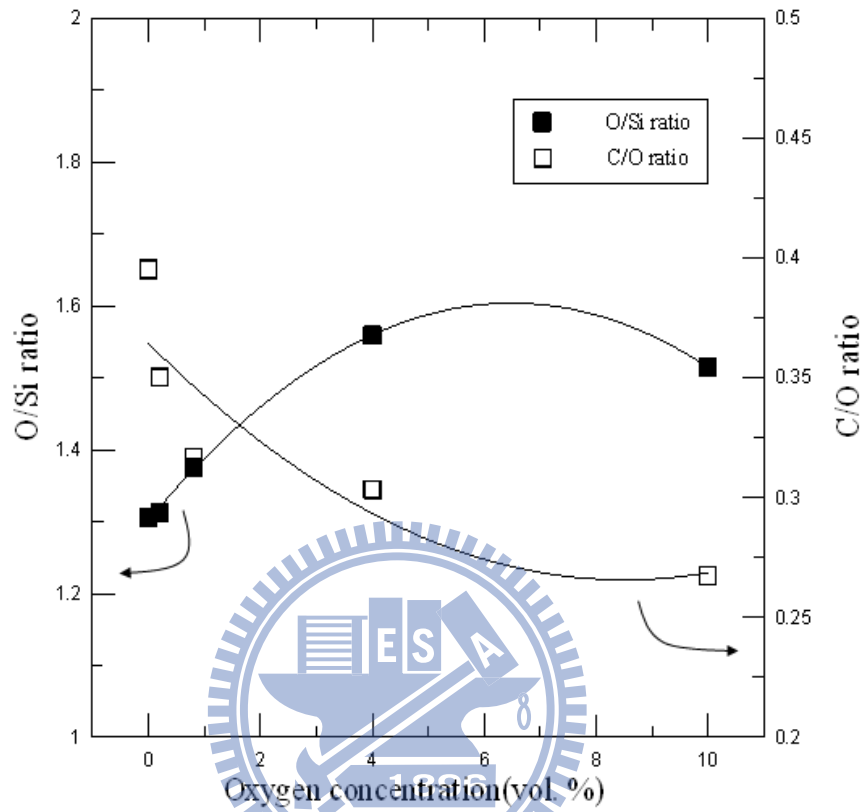


Figure 3.26 Evolution of oxygen to silicon ratio and carbon concentration of SiO_x thin films deposited at substrate temperature $200\text{ }^\circ\text{C}$ using argon plasma mixed with different oxygen concentrations (passes: 20).

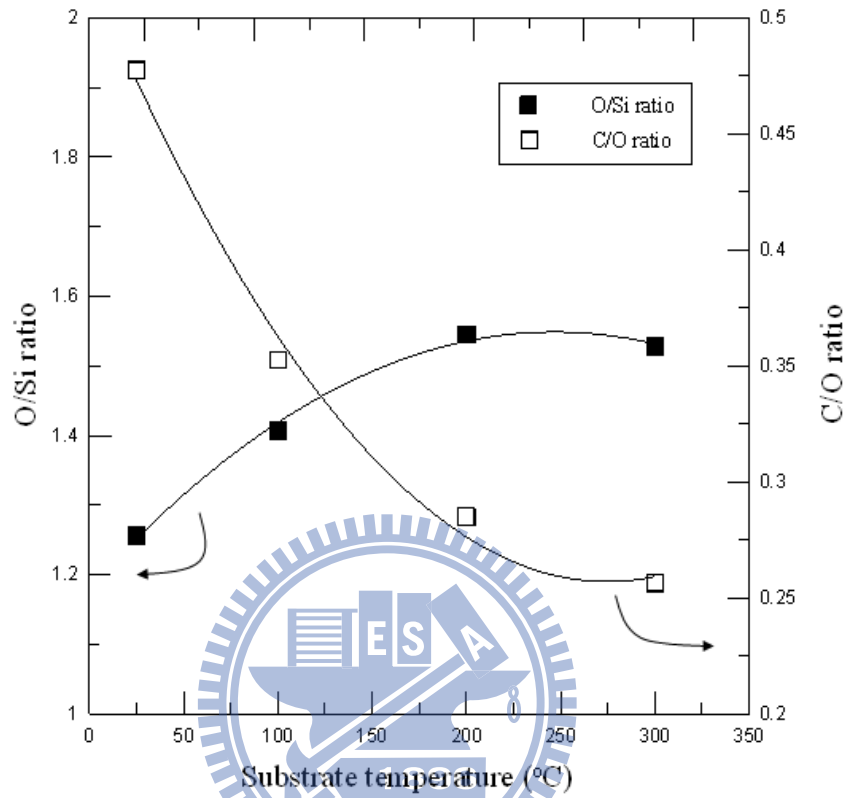


Figure 3.27 Evolution of oxygen to silicon ratio and carbon concentration of SiO_x thin films deposited at different substrate temperature (oxygen concentration: 4 %; passes:

20).



Figure 3.28 Image of super-hydrophobic surface.

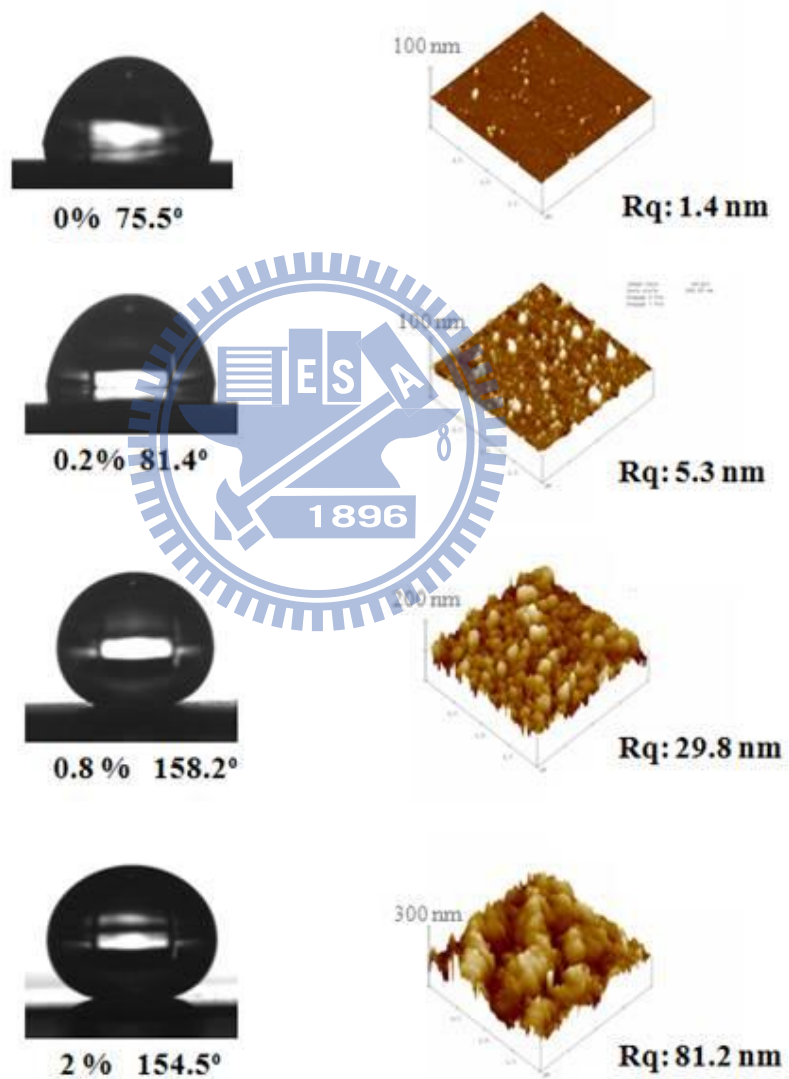


Figure 3.29 Change in the contact angle with the surface roughness (50W, 300 °C substrate temperature, 5 mm treatment distance and 60 treatment passes).